Changes in Histone Isoform Abundnance and Histone Post-Translational Modifications during Anoxia Tolerance and Recovery in WS40NE cells of *Austrofundulus limnaeus*

Chelsea Hughes[1,2], Elizabeth A. Mojica[3], Dietmar Kültz[3], Jason E. Podrabsky[1,4]

1. Department of Biology, Center for Life in Extreme Environments, Portland State University, P.O. Box 751, Portland, OR 97201, USA

2. Nicholas School of the Environment, Duke University, 308 Research Dr, Levine Science Research Center, Durham, NC 27708, USA

3. Department of Animal Sciences and Genome Center, University of California, Davis, One Shields Avenue, Meyer Hall, Davis, CA 95616, USA

4. Department of Integrative Biology, Oregon State University, 2701 SW Campus Way, Corvallis, OR 97331, USA

Keywords: mass spectrometry; epigenetics; histone post-translational modifications; anoxia; stress tolerance

Abstract

Anoxia is an often-lethal stressor to vertebrates, yet some vertebrates have adapted cellular mechanisms to survive in anoxic conditions. Embryos of the annual killifish *Austrofundulus limnaeus* have the greatest tolerance to anoxia of all vertebrates, yet the epigenetic mechanisms that support their anoxia tolerance are unknown. Using mass spectrometry, 1043 unique biologically relevant histone post-translational modifications (unimod+histone residue) were detected in WS40NE cells, representing thirteen types of biologically relevant histone post-translational modifications (hPTMs) present during normoxia, 1 d anoxia, 4 d anoxia, and aerobic recovery from anoxia. Of these 1043 hPTMs, 816 were significantly differentially expressed in at least one comparison. Thirty-six significant hPTMs were considered highly condition dependent. Additionally, at least four histone isoforms were differentially expressed, representing H2A, H2B, and H3 isoforms. Our data suggests that specific histone modifications as well as changes in histone isoform abundance in WS40NE cells may be necessary to successfully respond to extreme changes in oxygen availability.

Introduction

All organisms must respond to their environment, which offers both opportunities and threats. By changing which genes are expressed, organisms can modify their phenotype to take advantage of opportunities and neutralize threats. However, environmental stressors can often lead to aberrant gene expression in organisms that lack these adaptations. This is particularly true during anoxic stress in mammals, which can cause apoptosis and inappropriate reentry into the cell cycle in mammalian cells [1, 2]. Specifically in mammalian neurons, apoptosis is associated with cellular dysregulation that leads these terminally differentiated cells to re-enter the cell

37 cycle, which often leads to catastrophic cell failure [2]. Additionally, mitochondrial
38 dysregulation is associated with anoxia due to inhibition of the electron transport chain (ETC)
39 and depolarization of the inner mitochondrial membrane that can lead to apoptosis [3-5]. The
40 subsequent cell death causes tissue damage, which continues when oxygen is returned to the
41 affected area, a phenomenon known as ischemia-reperfusion injury in mammals [6]. Ischemia-
42 reperfusion increases reactive oxygen species (ROS) such as the superoxide anion (O^{-2}),
43 hydrogen peroxide (H_2O_2), and hydroxyl radical (OH^-) [7]. While low levels of ROS are a
44 normal byproduct of mitochondrial metabolism [8], high levels of ROS can lead to neuronal
45 death within 5 minutes [9, 10]. In contrast, a handful of vertebrates have adapted mechanisms to
46 modify their gene expression to survive environmental stressors, including osmotic, thermal,
47 ROS, and anoxia with little or no damage [11-19].Therefore, there is a need to understand how
48 gene expression is regulated in anoxia tolerant vertebrates to understand how they avoid these
49 fates. This study focuses on epigenetic histone modifications in response to anoxia in a cell line
50 isolated from anoxia-tolerant embryos of the annual killifish, *Austrofundulus limnaeus*.

51 Epigenetic responses to a variety of stressors are documented in multiple organisms [20-23].
52 However, few histone post-translational modifications (hPTMs) have been investigated in
53 response to hypoxia or anoxia. Additionally, these data often come from anoxia intolerant
54 organisms that are experiencing a disease state and are likely failing [24, 25]. Additionally, this
55 research often focuses only on well-known residues and specific types of hPTMs such as
56 methylation [26, 27]. For example, histone-3 lysine-4 trimethylation (H3K4me3) and
57 H3K36me3 are known to change in HeLa cells within 1 h of hypoxic exposure, but HeLa cells
58 begin to die within 1 d of severe hypoxia [28, 29]. Limited research exists on histone
59 modifications in anoxia tolerant organisms, but this work again focuses on well-known

60 modifications such as acetylation and methylation [30]. It is unknown how less studied hPTMs,
61 such as lactylation, 4-hydroxynonenal, and oxidation are impacted by anoxic stress, particularly
62 in anoxia tolerant species. Even better characterized hPTMs like ubiquitylation are not well
63 understood in anoxia. While ubiquitylation of the proteome has been studied in ischemia and
64 anoxia recovery [31, 32], to our knowledge, anoxia-induced histone ubiquitylation has never
65 been explored in a continuous cell line.

66 Embryos of the annual killifish *Austrofundulus limnaeus* have the greatest tolerance to anoxia of
67 all vertebrates, making them the ideal model to study the cellular mechanisms necessary for
68 anoxia tolerance. This remarkable tolerance of anoxia is supported by the ability of embryos to
69 arrest development and enter a state of anoxia-induced quiescence [33]. The global histone
70 landscape of developing embryos (Wourms' Stage 36) under normoxia and after 24 h of anoxia
71 suggests a stabilization of both histone isoform and hPTM abundance [34]. This is surprising, as
72 hPTMs are known to respond to stressors quickly [22, 28, 35, 36]. However, this stabilization
73 represents an averaged histone landscape for multiple cell types [34]. It is unclear how specific
74 cell lines of *A. limnaeus* respond to anoxia, particularly in the absence of tissue-dependent cell
75 signaling. Additionally, no research has investigated how the histone landscape of *A. limnaeus*
76 changes when exposed to longer bouts of anoxia or during recovery from anoxia.

77 PSU-AL-WS40NE (from now on WS40NE) is a neuroepithelial cell line that was isolated from
78 an embryonic (Wourms' Stage 40) *A. limnaeus* tissue explant. These cells can survive for at least
79 49 days without oxygen [37], while SH-SY5Y human neuroblastoma cells can survive anoxia for
80 only approximately 1.3 days [38], and mouse N2A cells can survive for just over 3 days [37].
81 Here, we describe for the first time the global histone landscape of WS40NE cells exposed to

82 anoxia and recovery from anoxia. We hypothesize cells undergo extensive changes to histone
83 isoforms and the hPTM landscape in response to anoxia and aerobic recovery from anoxia.

84 **Results**

85 ***Histone Abundance***

86 Our methods resulted in the identification of 1,927 peptides across at least twenty-three distinct
87 histone proteins based on their unique protein accession number. These proteins were
88 representative of H1, H2A, H2B, and H3 isoforms. No H4 isoforms were detected. Sequence
89 coverage ranged from 17-100% (Fig. 1). At least four histones were differentially expressed
90 across the four experimental time points (Fig. 1).

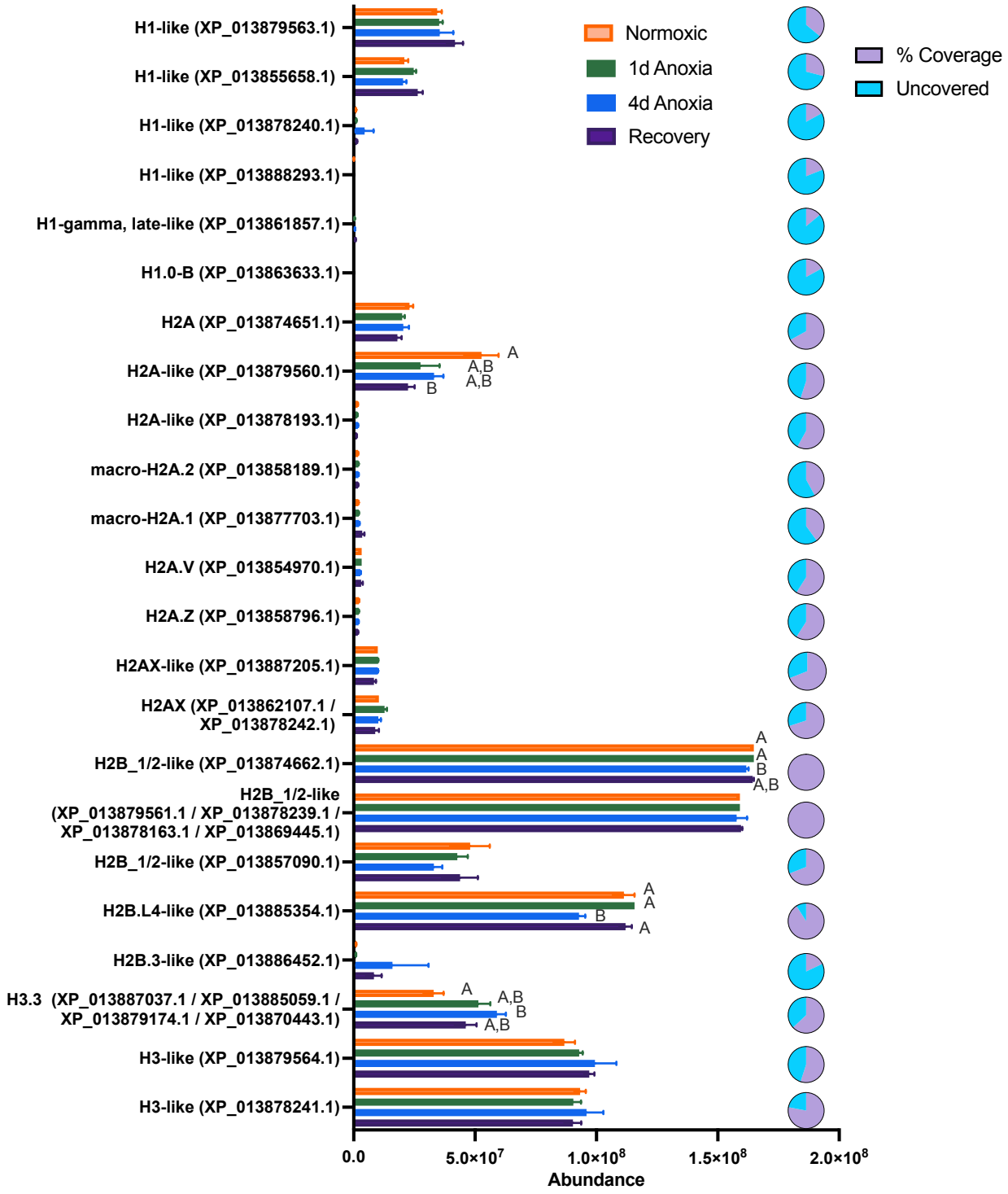

91

92 **Figure 1. Histone isoform abundance in WS40NE cells.** Twenty distinct histone proteins were identified based on

93 their unique protein accession number, as well as three groups of histones that could not be distinguished. Bar

94 graphs represent the quantile normalized mean ± SEM of histone relative abundance during normoxia (orange), 1 d
95 anoxia (green), 4 d anoxia (blue), and 1 d of recovery (dark purple). Letters over bars represent statistically
96 significant isoform abundances determined by pairwise comparisons. Pie charts represent the sequence coverage
97 (light purple) and the percent of peptide sequences that were not detected (blue) for each isoform. Sequence
98 coverage is defined as the total observed protein sequence length divided by the total protein length. Note that due to
99 different peptide ionization efficiencies, histone isoform abundance can only be compared across conditions and not
100 to one another within a condition.

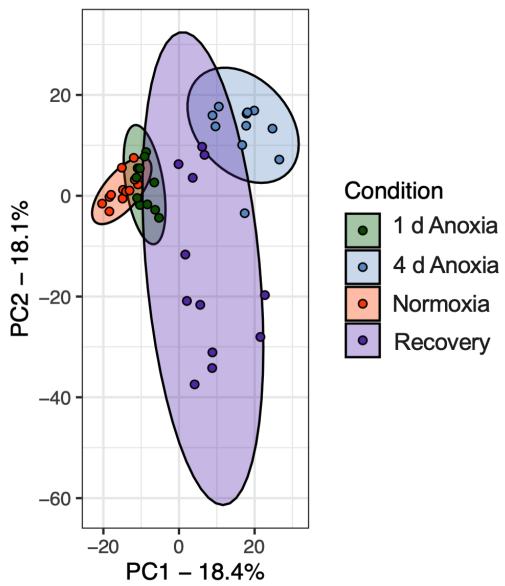

Histone H3.3 protein increased significantly within 4 d of anoxia, while an H2A-like protein decreased during anoxia compared to normoxia, decreasing significantly during recovery. Two histone H2B isoforms decreased in abundance after 4 d of anoxia. However, principal component analysis demonstrated broad sample similarity across conditions when considering the abundances of all histone isoforms (Fig. 2).

109 **Figure 2. Principal component analysis of histone isoform abundance in WS40NE cells exposed to anoxia and**
110 **aerobic recovery from anoxia.** The mean quantile normalized abundance values of all histone isoforms were used
111 to construct a PCA Plot. Normoxic (purple), 1 d anoxic (green), 4 d anoxic (blue), and recovery samples (pale blue)
112 are plotted according to PC1 and PC2 with a 95% confidence ellipse surrounding each cluster.

113 ***Histone Post-translational Modifications***

114 Post-translational modifications were evaluated in a residue-specific manner to determine
115 specific sites of differential modification on each histone. Principal component analysis (PCA)
116 illustrates that, globally, the hPTM landscape is most unique after 4 d of anoxia compared to
117 normoxia (Fig. 3C). It is worth noting the high variation in PC2 for the recovery time point (Fig.

118 3C). Out of 1293 unique hPTMs detected, 1043 unique hPTMs (hPTM type+residue) were
119 considered biologically relevant, representing thirteen types of biologically relevant PTMs (Fig.
120 3A,B). Four hundred and sixty-one residues were modified with biologically relevant hPTMs,
121 with many residues being modified with multiple types of hPTMs. These types of modifications
122 included commonly studied modifications such as acetylation, methylation, phosphorylation, and
123 ubiquitylation, and less studied modifications such as lactylation and 4-hydroxynonenal. All
124 thirteen types of modifications were statistically significant on at least one residue in at least one
125 comparison, with oxidation/hydroxylation and dioxidation having the greatest number of
126 significantly modified residues, followed closely by dehydration and phosphorylation (Fig. 3A).
127 As expected, the percent sequence coverage is positively correlated with the number of
128 significant hPTMs (Fig. 3D, $r = 0.7$, $p = 0.0003$), and thus for certain histones our ability to draw
129 global conclusions is somewhat limited. However, several isoforms, such as H1-like
130 (XP_013879563.1), do not follow this trend, suggesting these are highly modified isoforms (Fig.
131 3D). Of the unique biologically relevant PTMs detected, 816 were significant in at least one
132 comparison (Fig. 3E). Hundreds of significant differential hPTMs were present across all four
133 timepoints with 4 d of anoxia having the highest number compared to other time points (Fig. 3E).

134

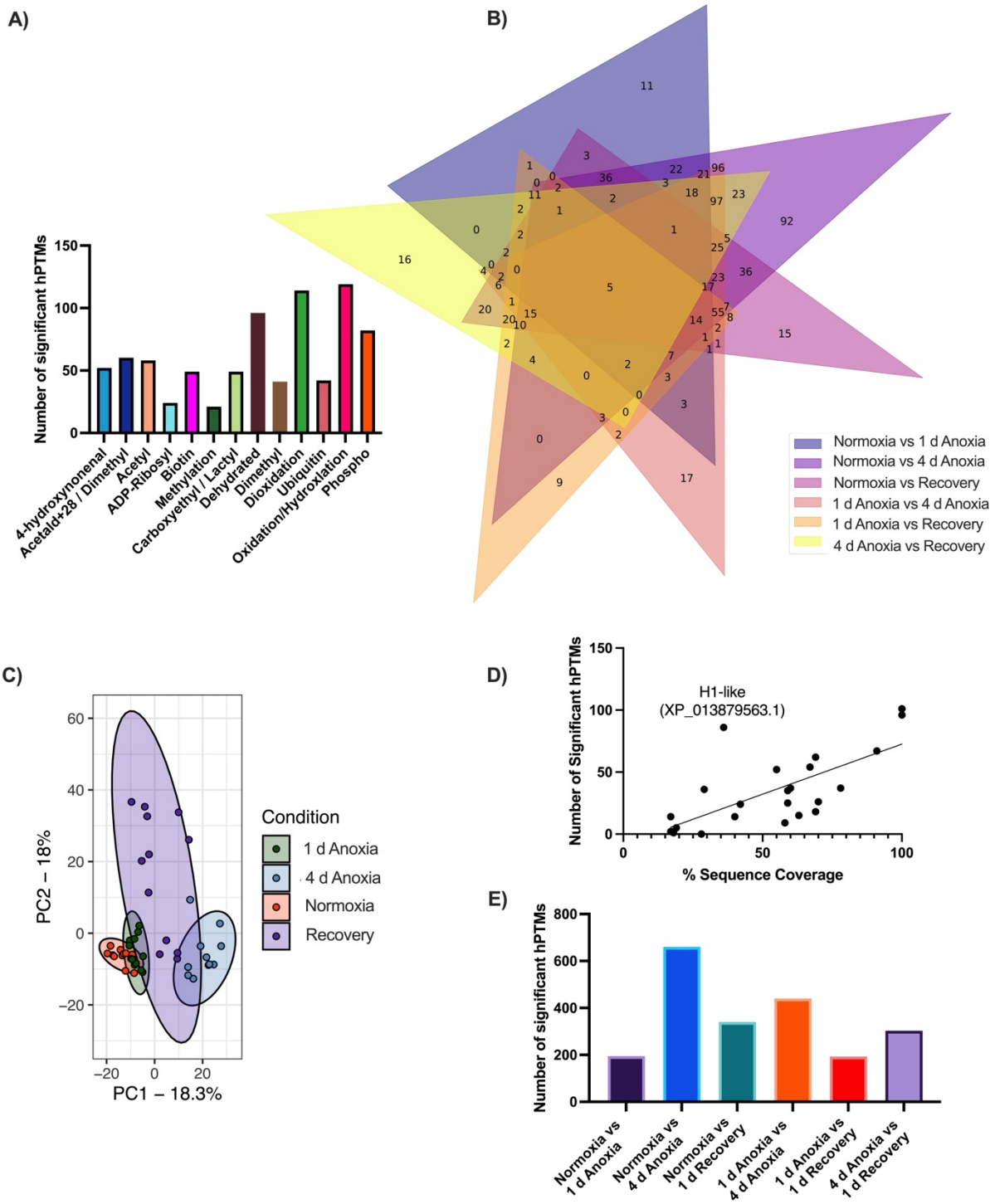
A)
Number of significant hPTMs
150
100
50
0
4-hydroxynonenal
Acetald+28 / Dimethyl
Acetyl
ADP-Ribosyl
Biotin
Methylation
Carboxyethyl / Lactyl
Dehydrated
Dimethyl
Dioxidation
Ubiquitin
Oxidation/Hydroxlation
Phospho
B)
Normoxia vs 1 d Anoxia
Normoxia vs 4 d Anoxia
Normoxia vs Recovery
1 d Anoxia vs 4 d Anoxia
1 d Anoxia vs Recovery
4 d Anoxia vs Recovery
C)
PC2 – 18%
PC1 – 18.3%
Condition
1 d Anoxia
4 d Anoxia
Normoxia
Recovery
D)
Number of Significant hPTMs
H1-like
(XP_013879563.1)
% Sequence Coverage
E)
Number of significant hPTMs
Normoxia vs 1 d Anoxia
Normoxia vs 4 d Anoxia
Normoxia vs 1 d Recovery
1 d Anoxia vs 4 d Anoxia
1 d Anoxia vs 1 d Recovery
4 d Anoxia vs 1 d Recovery

135

136 **Figure 3. Quantification of global patterns of significant histone post-translational modifications in WS40NE**
137 **cells exposed to anoxia and recovery from anoxia. (A)** The number of hPTMs with statistically significant
138 changes in abundance were plotted by modification type across all histone isoforms**. (B)** Venn diagram illustrating
139 the occurrence of the 297 unique and biologically-relevant hPTMs across the experimental conditions used in this
140 study. The Venn diagram is schematic and non-proportional. The numbers within each colored section indicate the
141 number of significantly differentially expressed histone modifications shared among the indicated pairwise
142 comparisons. **(C)** PCA plot of the M-values of all hPTMs indicate that hPTM patterns at 4 d of anoxia are unique
143 compared to the other experimental conditions. It is also noteworthy that variation in global patterns of hPTMs
144 appears to be high during aerobic recovery. Individual samples (data points) are surrounded by 95% confidence
145 ellipses for each treatment group. **(D)** There is a positive correlation ($r = 0.7$, $p = 0.0003$) between percent sequence
146 coverage for each histone isoform and the number of significant hPTMs identified. However, several isoforms do
147 not follow this trend, suggesting these are highly modified isoforms. **(E)** The bar graph represents the number of
148 significantly expressed hPTMs in each t-test comparison.

149 Thirty hPTMs were highly abundant (having an average relative abundance of 50% or greater)
150 across all conditions. Of the high abundance hPTMs, 15 displayed an average relative abundance
151 across all samples of exactly 100% during all conditions, meaning that each specific residue was
152 always modified by that PTM (Table 1). Five histones had at least one hPTM site with 100%
153 relative abundance, representing H1, H2A, and H3 histones. At least 8 distinct types of PTMs are
154 represented in this group with dehydration accounting for 30% of these stable modifications.

155

156 **Table 1. Histone post-translational modifications with 100% relative abundance in WS40NE cells.** Fifteen
157 hPTMs, across 5 histone isoforms, always occurred at the same residue across all experimental conditions. At least
158 eight distinct types of PTMs are represented.
159

160

Protein Accession	Protein Description	Amino Acid + Position	PTM Description
XP_013861857.1	H1-gamma,_late-like	196K	Acetylation
XP_013861857.1	H1-gamma,_late-like	175K	Biotinylation
XP_013861857.1	H1-gamma,_late-like	173P	Oxidation/Hydroxylation
XP_013861857.1	H1-gamma,_late-like	191K	Acetylation
XP_013861857.1	H1-gamma,_late-like	157K	Acetylation
XP_013861857.1	H1-gamma,_late-like	228K	Dioxidation
XP_013861857.1	H1-gamma,_late-like	24R	4-hydroxynonenal
XP_013861857.1	H1-gamma,_late-like	46S	Phosphorylation
XP_013878240.1	H1-like	64S	Dehydrated
XP_013885354.1	H2B.L4-like	46S	Dehydrated
XP_013885354.1	H2B.L4-like	55S	Dehydrated
XP_013885354.1	H2B.L4-like	43T	Dehydrated
XP_013885354.1	H2B.L4-like	31Y	Dehydrated
XP_013878241.1	H3-like	24R	Oxidation/Hydroxylation
XP_013878241.1	H3-like	17K	Oxidation/Hydroxylation

161 Individual hPTMs at specific residues were also evaluated, and the most condition-dependent
162 hPTMs were identified. Significant differential modifications were detected on all groups of
163 histones (H1, H2A, H2B, H3), with H1-gamma late-like (XP_013861857.1) being the only
164 isoform that did not have any significant hPTMs detected. Thirty-seven hPTMs were considered
165 highly condition dependent, being significantly differentially expressed across 5-6 comparisons
166 (Table 2).
167
168 **Table 2. Highly condition-dependent histone post-translational modifications in WS40NE cells exposed to**
169 **anoxia and aerobic recovery from anoxia.** To be considered highly condition-dependent, hPTMs had to be
170 significant across at least 5 of 6 different comparisons. Thirty-seven hPTMs were selected as the most condition
171 dependent. Differential modifications of histone residues were evaluated using a two-tailed t-test with the
172 Benjamini-Hochberg correction applied to account for multiple hypothesis testing.
173

Protein Accession	Protein Description	Amino Acid + Position	PTM Description
XP_013863633.1	H1.0-B	25K	Acetylation
XP_013863633.1	H1.0-B	19K	4-hydroxynonenal
XP_013879563.1	H1-like	17K	Acetylation
XP_013879563.1	H1-like	51K	4-hydroxynonenal
XP_013879563.1	H1-like	63S	Phosphorylation
XP_013879563.1	H1-like	62R	Oxidation/Hydroxyl
XP_013878193.1	H2A-like	102S	Dehydration
XP_013879560.1	H2A-like	123K	Carboxyethyl/ lactylation
XP_013854970.1	H2A.V	116K	Oxidation/hydroxylation
XP_013854970.1	H2A.V	121K	Biotinylation

XP_013854970.1	H2A.V	122K	Dioxidation
XP_013885354.1	H2B.L4-like	74Y	Phosphorylation
XP_013885354.1	H2B.L4-like	78S	Ubiquitylation
XP_013885354.1	H2B.L4-like	79T	Dehydration
XP_013885354.1	H2B.L4-like	79T	Phosphorylation
XP_013885354.1	H2B.L4-like	82S	Dehydration
XP_013885354.1	H2B.L4-like	83R	Oxidation/hydroxylation
XP_013885354.1	H2B.L4-like	116K	Methylation
XP_013879561.1 /			
XP_013878239.1 /			
XP_013878163.1 /			
XP_013869445.1	H2B_1/2	41Y	Phosphorylation
XP_013879561.1 /			
XP_013878239.1 /			
XP_013878163.1 /			
XP_013869445.1	H2B_1/2	84K	4-hydroxynonenal
XP_013879561.1 /			
XP_013878239.1 /			
XP_013878163.1 /			
XP_013869445.1	H2B_1/2	89T	Phosphorylation
XP_013879561.1 /			
XP_013878239.1 /			
XP_013878163.1 /			
XP_013869445.1	H2B_1/2	90S	Dehydration
XP_013879561.1 /			
XP_013878239.1 /			
XP_013878163.1 /			
XP_013869445.1	H2B_1/2	90S	Phosphorylation

XP_013879561.1 /			
XP_013878239.1 /			
XP_013878163.1 /			
XP_013869445.1	H2B_1/2	114T	Dehydration
XP_013879561.1 /			
XP_013878239.1 /			
XP_013878163.1 /			
XP_013869445.1	H2B_1/2	124K	Methylation
XP_013857090.1	H2B_1/2-like	41Y	Phosphorylation
XP_013857090.1	H2B_1/2-like	78R	Dioxidation
XP_013857090.1	H2B_1/2-like	81H	4-hydroxynonenal
XP_013857090.1	H2B_1/2-like	84K	Acetald+28 / Dimethylation
XP_013874662.1	H2B_1/2	35S	Phosphorylation
XP_013874662.1	H2B_1/2	41Y	Phosphorylation
XP_013874662.1	H2B_1/2	55S	Phosphorylation
XP_013874662.1	H2B_1/2	63S	Ubiquitylation
XP_013874662.1	H2B_1/2	86S	Phosphorylation
XP_013874662.1	H2B_1/2	89T	Phosphorylation
XP_013874662.1	H2B_1/2	90S	Phosphorylation
XP_013874662.1	H2B_1/2	124K	Methylation

Globally, hPTMs did not cover the majority of the residues that are theoretically available. Lysine residues were the most modified with 48.7-51.4% of the available residues modified across the different experimental conditions (Fig. 4A). The modification of specific amino acid residues varied based on experimental conditions (Fig. 4A). Lysines had the most types of modifications, with 10 distinct hPTMs detected globally, and of these, oxidation/hydroxylation, dioxidation, and acetylation were the most common (Fig. 4A). Serine (S) had the second most

181 types of modifications, with 5 distinct hPTMs occurring globally; dehydration and
182 phosphorylation dominated serine modifications (Fig. 4A). Globally, there were significant
183 changes in all types of hPTMs across all six comparisons (Fig. 4B,C): (a) 5 comparing normoxia
184 to 24 h anoxia, (b) 12 comparing normoxia to 4 d anoxia, (c) 8 comparing normoxia to 24 h
185 recovery,(d) 6 comparing 24 h anoxia to 4 d anoxia, (e) 4 comparing 24 h anoxia to 24 h
186 recovery, and (f) 2 comparing 4 d anoxia to 24 h recovery. The majority of the most common
187 modifications decreased significantly during anoxia and remained low even after 24 h of aerobic
188 recovery (Fig. 4B,C). Notably, acetylation, dehydration, oxidation, and dioxidation all increase
189 during anoxia. (Fig. 4B,C).
190

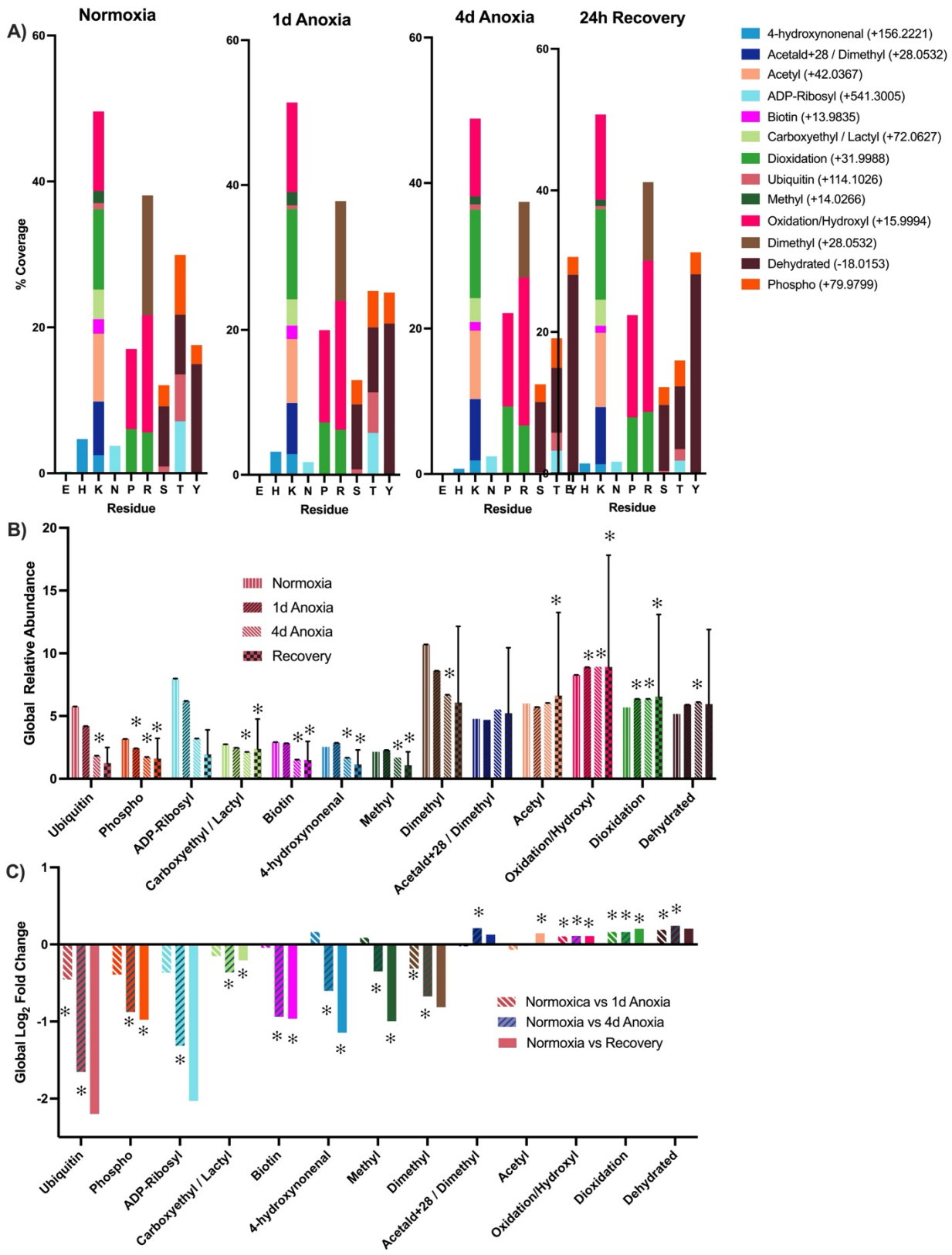
A)
Normoxia
1d Anoxia
4d Anoxia
24h Recovery
% Coverage
Residue
E H K N P R S T Y
4-hydroxynonenal (+156.2221)
Acetald+28 / Dimethyl (+28.0532)
Acetyl (+42.0367)
ADP-Ribosyl (+541.3005)
Biotin (+13.9835)
Carboxyethyl / Lactyl (+72.0627)
Dioxidation (+31.9988)
Ubiquitin (+114.1026)
Methyl (+14.0266)
Oxidation/Hydroxyl (+15.9994)
Dimethyl (+28.0532)
Dehydrated (-18.0153)
Phospho (+79.9799)
B)
Global Relative Abundance
Normoxia
1d Anoxia
4d Anoxia
Recovery
Ubiquitin
Phospho
ADP-Ribosyl
Carboxyethyl / Lactyl
Biotin
4-hydroxynonenal
Methyl
Dimethyl
Acetald+28 / Dimethyl
Acetyl
Oxidation/Hydroxyl
Dioxidation
Dehydrated
C)
Global Log2 Fold Change
Normoxica vs 1d Anoxia
Normoxia vs 4d Anoxia
Normoxia vs Recovery

191

192 **Figure 4. Global changes in the histone PTM landscape of WS40NE cells during anoxia and aerobic recovery**
193 **from anoxia. (A)** Thirteen types of hPTMs were detected across nine types of amino acid residues in WS40NE
194 cells. The average mass as reported by Unimod is listed beside each PTM. While most residue types are unmodified,
195 lysine (K) residues were the most consistently modified (54.7 - 58.3%) across the different experimental conditions.
196 **(B)** An ANOVA with Dunnett's multiple comparison test applied was used to determine significance of all
197 conditions compared to normoxia (error bars represent standard deviation). From a global perspective, the
198 abundance of most hPTMs decreases in response to anoxia and fails to return to normoxic values after 1 d of aerobic
199 recovery. Acetylation, oxidation, dioxidation and dehydration increase modestly in response to anoxia. **(C)** Fold
200 change data were calculated from the global mean abundance data for each hPTM. A two-tailed t-test was used to
201 compare the relative abundance of hPTMs in all conditions with the Benjamini-Hochberg correction applied to
202 account for multiple hypothesis testing.
203

204 ***Characterization of histone H1***

205 Six H1 proteins were identified: (**A**) H1-like (XP_013879563.1), (**B**) H1-like
206 (XP_013855658.1), (**C**) H1-like (XP_013878240.1), (**D**) H1-like (XP_013888293.1), (**E**) H1-
207 gamma late-like (XP_013861857.1), and (**F**) H1.0-B (XP_013863633.1). Thirteen types of
208 PTMs were identified across these isoforms (Figs. 5A). Interestingly, H1-like (XP_013879563.1)
209 appears to carry more modifications compared to the other isoforms even when percent coverage
210 is taken into account (Figs. 1, 3D, 5C). Nine of the 15 modifications with an average relative
211 abundance of exactly 100% in all samples are H1 isoforms, with H1-gamma late-like
212 (XP_013861857.1) having 8 of the 10 (Table 1).
213

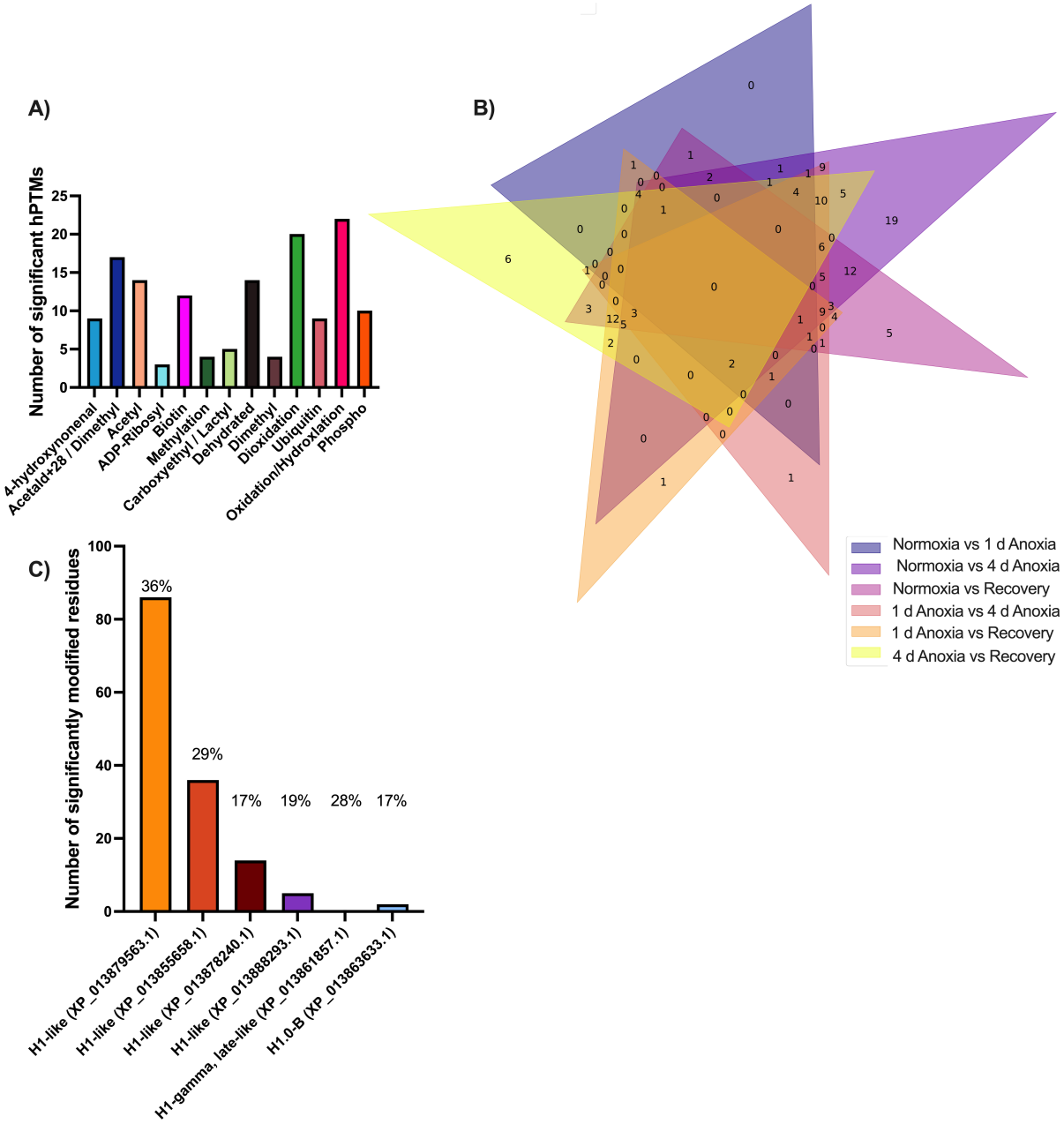

Figure 5. Significant differential histone post-translational modifications on histone H1 isoforms in WS40NE cells. (**A**) The most commonly significant differential hPTM across H1 isoforms were oxidation (22 hPTMs), dioxidation (20 hPTMs), and acetald+28/dimethylation (17 hPTMs). (**B**) Venn diagram illustrating the occurrence of unique and biologically-relevant hPTMs on H1 histone isoforms across experimental treatment groups. The Venn diagram is schematic and non-proportional. The numbers within each colored section indicate the number of significantly differentially expressed histone modifications shared among the indicated pairwise comparisons. (**C**) Five of the six H1 histone isoforms had residues with significantly different hPTM modifications in response to

222 anoxia. The percentage above each bar represents the peptide sequence coverage of that isoform. Note that H1-
223 gamma late-like is modified, but those modifications are stable across experimental treatment groups.
224
225 All six H1 isoforms had residues with significant hPTM modifications, while 5 isoforms had at
226 least one hPTM that changed in relative abundance in response to experimental treatments. One
227 hundred and forty-three significant hPTMs were present on H1 isoforms in at least one condition
228 (Fig. 5). The most common differential modifications in response to the experimental treatments
229 across H1 isoforms were oxidation (22 significant unique hPTMs), dioxidation (20 significant
230 unique hPTMs), and acetald+28/dimethylation (17 significant unique hPTMs) (Fig. 5). Six
231 highly condition-dependent hPTMs were significant across five different comparisons: H1-like
232 (XP_013879563.1) 17K acetylation, 62R oxidation/hydroxylation, and 63S phosphorylation; H1-
233 like (XP_013855658.1) 51K 4-hydroxynonenal; and H1.0-B (XP_013863633.1) 19K 4-
234 hydroxynonenal and 25K acetylation (Fig. 6 and Table 2).
235

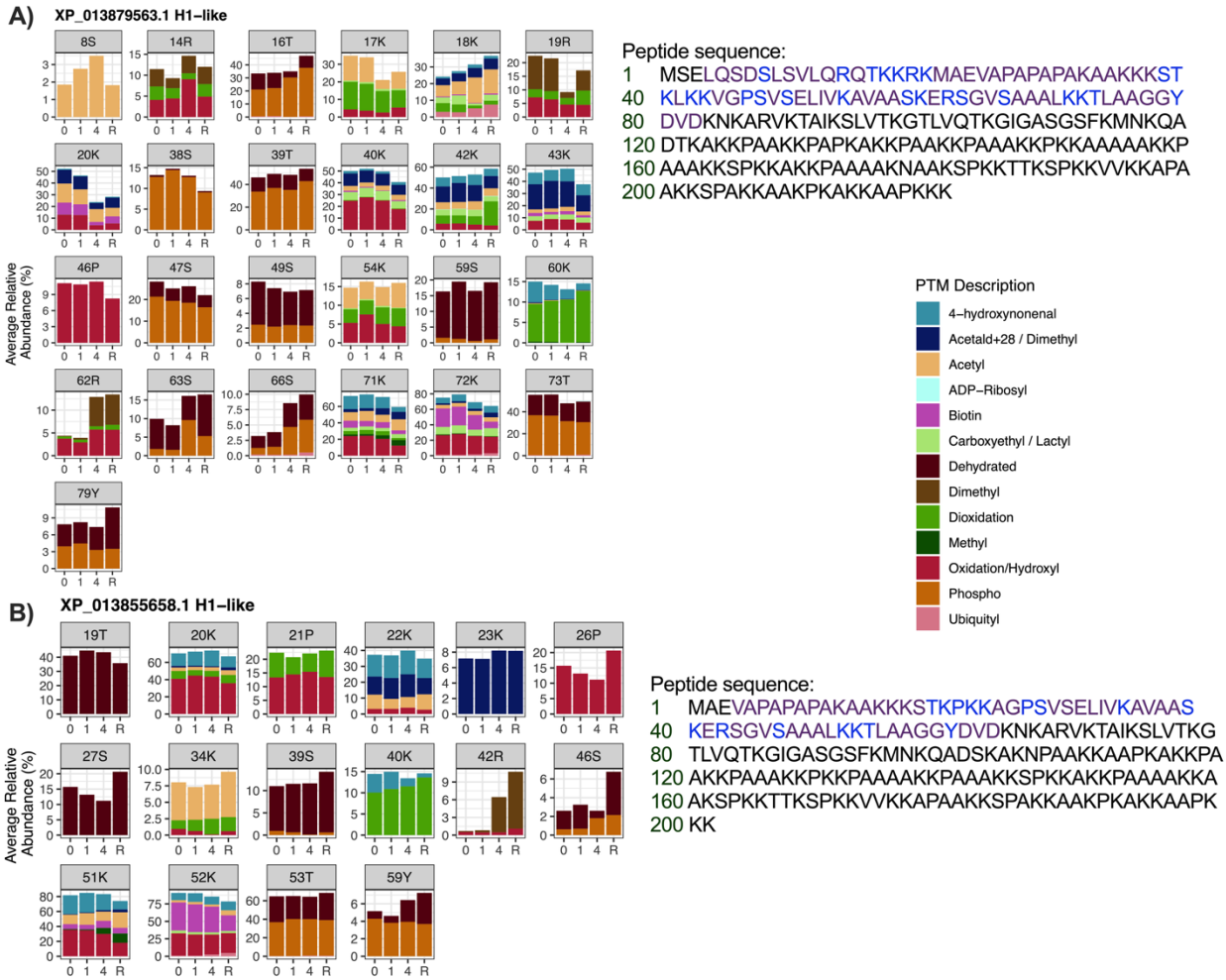
A)
XP_013879563.1 H1−like
8S
14R
16T
17K
18K
19R
20K
38S
39T
40K
42K
43K
46P
47S
49S
54K
59S
60K
62R
63S
66S
71K
72K
73T
79Y
Average Relative Abundance (%)
0 1 4 R
Peptide sequence:
1 MSELQSDSLSVLQRQTKKRKMAEVAPAPAPAKAAKKKST
40 KLKKVGPSVSELIVKAVAASKERSGVSAAALKKTLAAGGY
80 DVDKNKARVKTAIKSLVTKGTLVQTKGIGASGSFKMNKQA
120 DTKAKKPAAKKPAPKAKKPAAKKPAAAKKPKKAAAAAKKP
160 AAAKKSPKKAKKPAAAAKNAAKSPKKTTKSPKKVVKKAPA
200 AKKSPAKKAAKPKAKKAAPKKK
PTM Description
4−hydroxynonenal
Acetald+28 / Dimethyl
Acetyl
ADP−Ribosyl
Biotin
Carboxyethyl / Lactyl
Dehydrated
Dimethyl
Dioxidation
Methyl
Oxidation/Hydroxyl
Phospho
Ubiquityl
B)
XP_013855658.1 H1−like
19T
20K
21P
22K
23K
26P
27S
34K
39S
40K
42R
46S
51K
52K
53T
59Y
Average Relative Abundance (%)
0 1 4 R
Peptide sequence:
1 MAEVAPAPAPAKAAKKKSTKPKKAGPSVSELIVKAVAAS
40 KERSGVSAAALKKTLAAGGYDVDKNKARVKTAIKSLVTKG
80 TLVQTKGIGASGSFKMNKQADSKAKNPAAKKAAPKAKKPA
120 AKKPAAAKKPKKPAAAAKKPAAAKKSPKKAKKPAAAAKKA
160 AKSPKKTTKSPKKVVKKAPAAKKSPAKKAAKPKAKKAAPK
200 KK

236

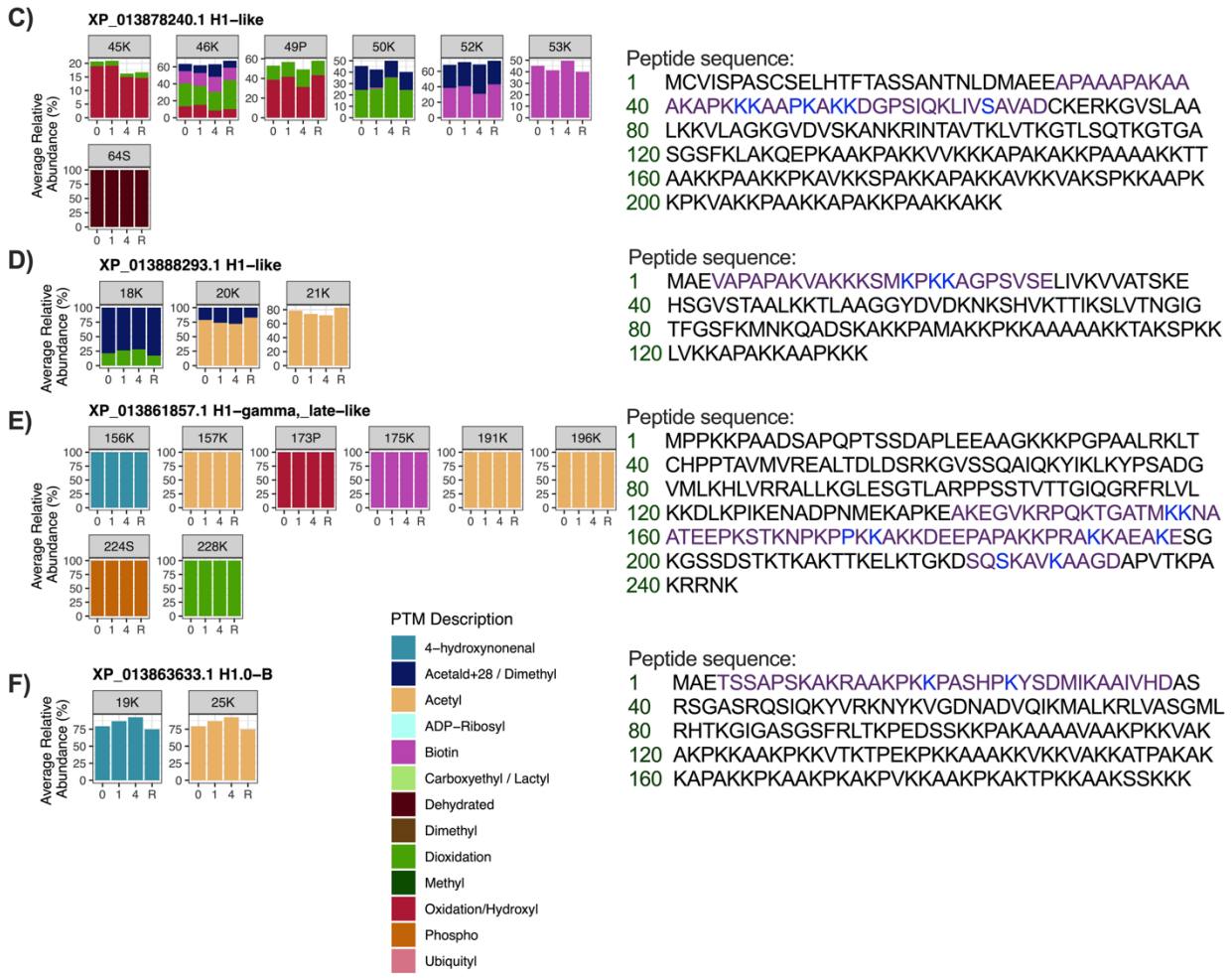

Figure 6. Characterization of post-translational modifications on Histone H1 isoforms in WS40NE cells exposed to anoxia and aerobic recovery from anoxia. Isoforms represented are (**A**) H1-like (XP_013879563.1), (**B**) H1-like (XP_013855658.1), (**C**) H1-like (XP_013878240.1), (**D**) H1-like (XP_013888293.1), (**E**) H1-gamma late-like (XP_013861857.1), and (**F**) H1.0-B (XP_013863633.1). Each panel represents a different amino acid position where at least one hPTM was detected. Amino acid residues are abbreviated using their one letter code. The x-axis displays the condition of the samples: 0 d in anoxia (0), 1 d in anoxia (1), 4 d in anoxia (4), or 1 d of aerobic recovery from 4 d of anoxia (R). The y-axis scales differ across panels to better visualize changes in low abundance hPTMs. Detected (purple) and modified (blue) peptides and the entire peptide sequences for each isoform are listed beside the panels. On each row, the number of the corresponding residue is listed in green.

Characterization of histone H2A

248 Nine H2A proteins were identified: (**A**) H2A (XP_013874651.1), (**B**) H2A-like
249 (XP_013879560.1), (**C**) H2A-like (XP_013878193.1), (**D**) macro-H2A.2 (XP_013858189.1), (**E**)
250 core histone macro-H2A.1 (XP_013877703.1), (**F**) H2A.V (XP_013854970.1), (**G**) H2A.Z
251 (XP_013858796.1), (**H**) H2AX-like (XP_013887205.1), and (**I**) H2AX-like (XP_013862107.1/
252 XP_013878242.1). Thirteen types of PTMs were identified across these isoforms (Fig. 7A) with
253 257 hPTMs significantly differentially abundant on H2A isoforms in at least one condition (Fig.
254 7B). All nine H2A isoforms had residues with significant hPTM modifications, with H2A
255 (XP_013874651.1) and H2A-like (XP_013879560.1) appearing to have a high proportion of
256 hPTMs for their percent coverage in the data (Fig. 7C). The top three most common hPTMs that
257 were significantly different in abundance in response to experimental treatments across H2A
258 isoforms were dioxidation (45 significant unique hPTMs), oxidation (38 significant unique
259 hPTMs), and dehydration (25 significant unique hPTMs) (Fig. 7A). Two highly condition-
260 dependent hPTMs were significantly different across six different comparisons: H2A-like
261 (XP_013879560.1) 123K carboxyethylation/lactylation (Figs. 7E, 8B) and H2A-like
262 (XP_013878193.1) 102S dehydration (Figs. 7D, 8C). Two additional highly condition-dependent
263 hPTMs were significantly different across five different comparisons: H2A.V
264 (XP_013854970.1)121K biotinylation and 122K dioxidation (Fig. 9A, Table 2).

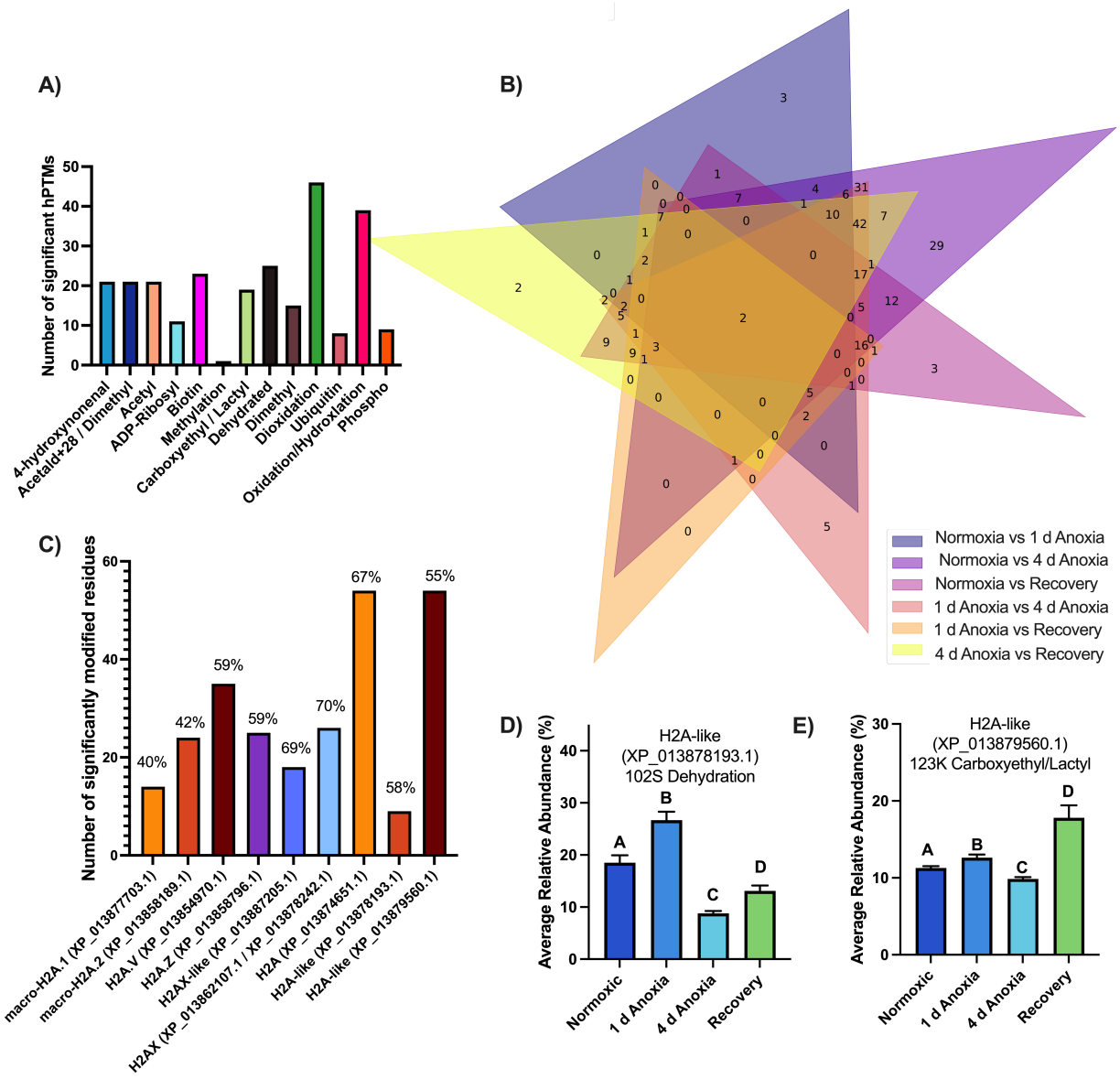

Figure 7. Significant differential post-translational modifications on histone H2A isoforms in WS40NE cells exposed to anoxia and aerobic recovery from anoxia. (A) The top three most commonly significant differential hPTMs across histone H2A isoforms were dioxidation (45 hPTMs), oxidation (38 hPTMs), and dehydration (25 hPTMs). (**B**) Venn diagram illustrating the occurrence of unique and biologically-relevant hPTMs on H2A histone isoforms across experimental treatment groups. The Venn diagram is schematic and non-proportional. The numbers within each colored section indicate the number of significantly differentially expressed histone modifications shared among the indicated pairwise comparisons. (**C**) At least nine H2A isoforms had residues that were

significantly modified. The percentage above each bar represents the peptide sequence coverage of that isoform. Note that two isoforms appear to be highly modified based on their percent sequence coverage. Two specific hPTMs were significant across all six pairwise comparisons: **(D)** H2A-like (XP_013878193.1) 102S dehydration and **(E)** H2A-like (XP_013879560.1) 123K carboxyethylation/lactylation. Bars represent means ± SEM (n=11-12).

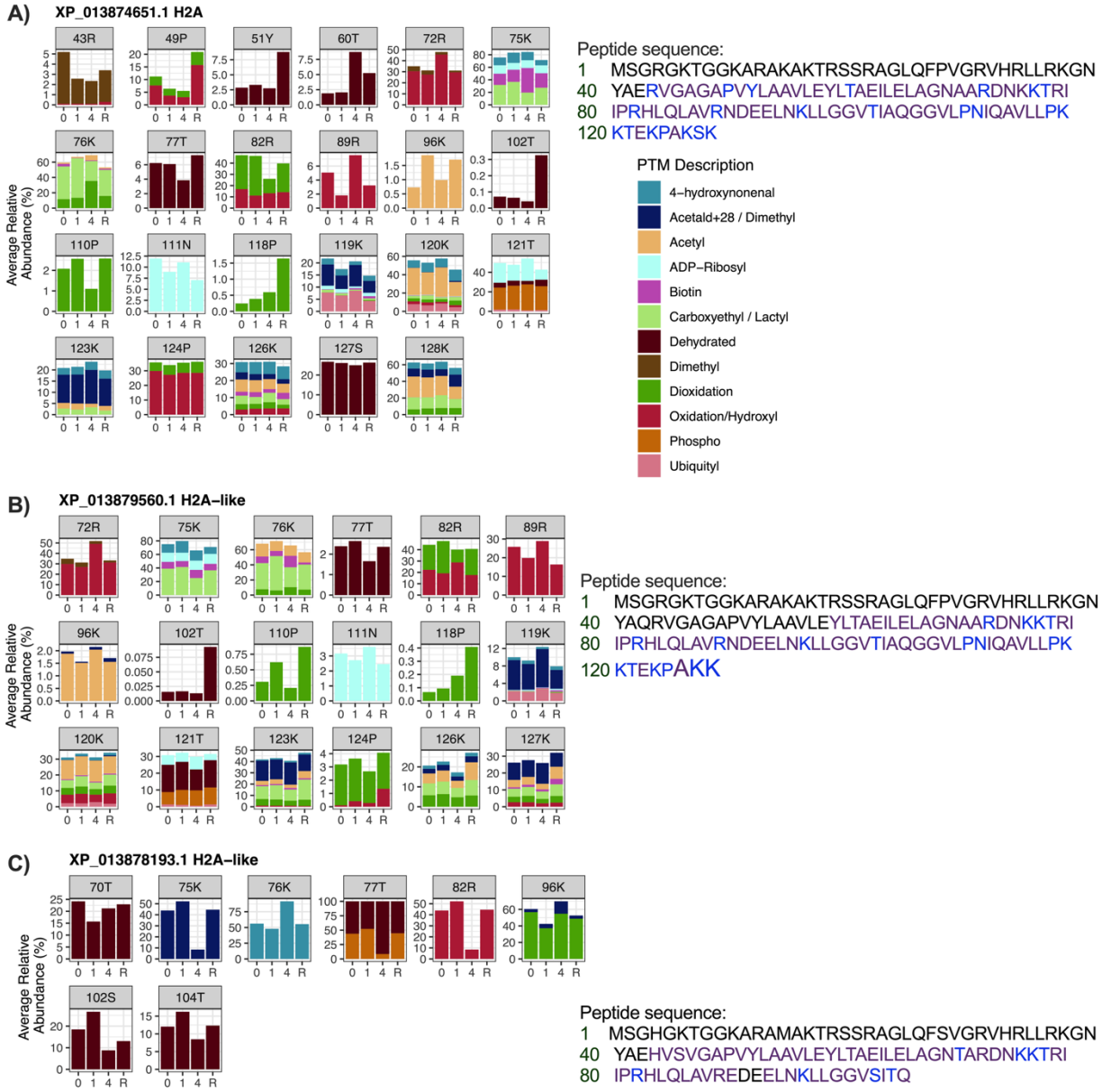

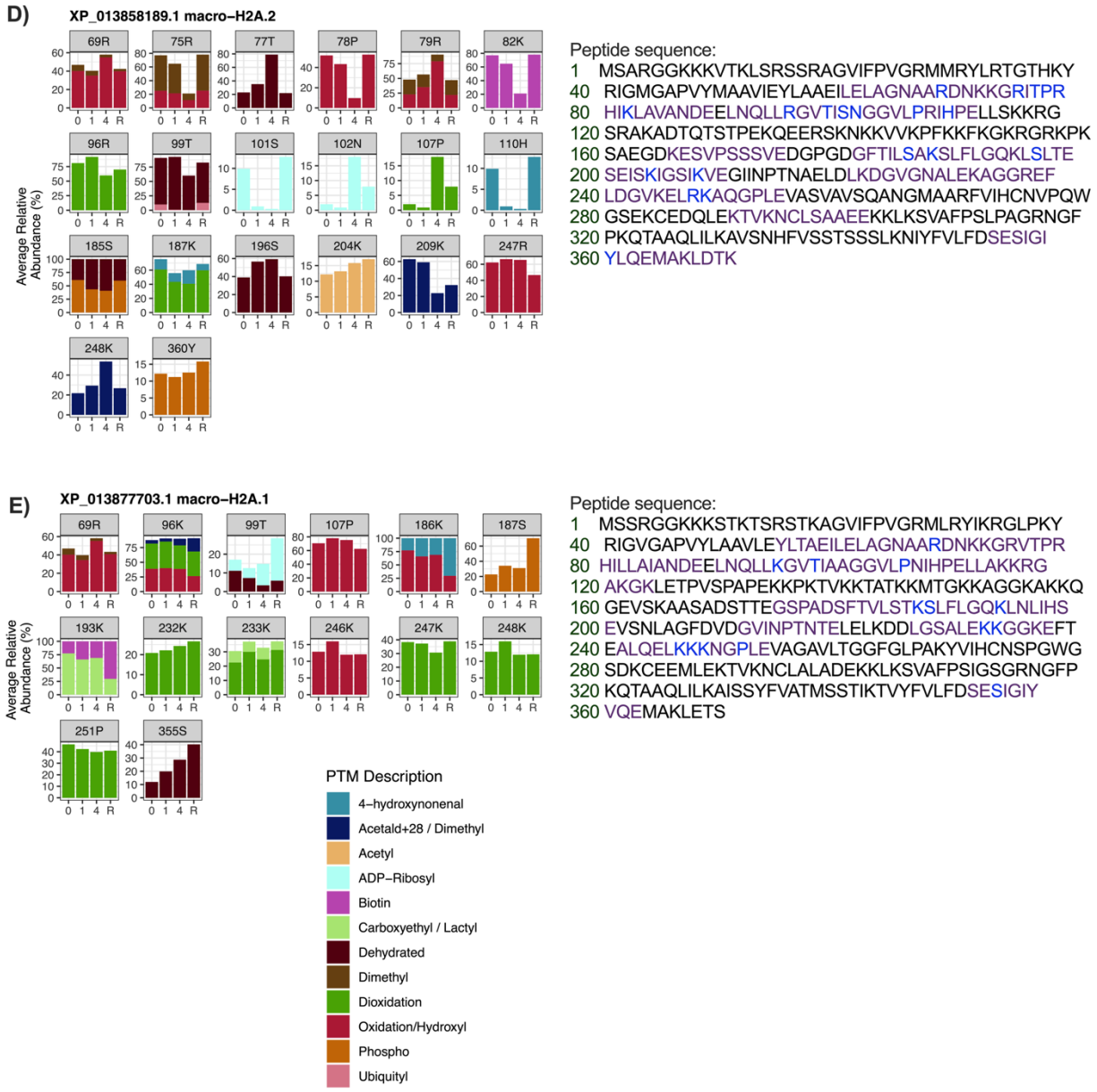

Figure 8. Characterization of the post-translational modifications on histone H2A isoforms in WS40NE cells exposed to anoxia and aerobic recovery from anoxia. Isoforms represented are (**A**) H2A (XP_013874651.1), (**B**)

281 H2A-like (XP_013879560.1), (**C**) H2A-like (XP_013878193.1), (**D**) macro-H2A.2 (XP_013858189.1), and (**E**)
282 macro-H2A.1 (XP_0138777031.1). Each panel represents a different amino acid position where at least one hPTM
283 was detected. Amino acid residues are abbreviated using their one letter code. The x-axis displays the condition of
284 the samples: 0 d in anoxia (0), 1 d in anoxia (1), 4 d in anoxia (4), or 1 d of aerobic recovery after 4 days in anoxia
285 (R). The y-axis scales differ across panels to better visualize changes in low abundance hPTMs. Detected (purple)
286 and modified (blue) peptides and the entire peptide sequences are listed beside the panels. On each row, the number
287 of the corresponding residue is listed in green.

288

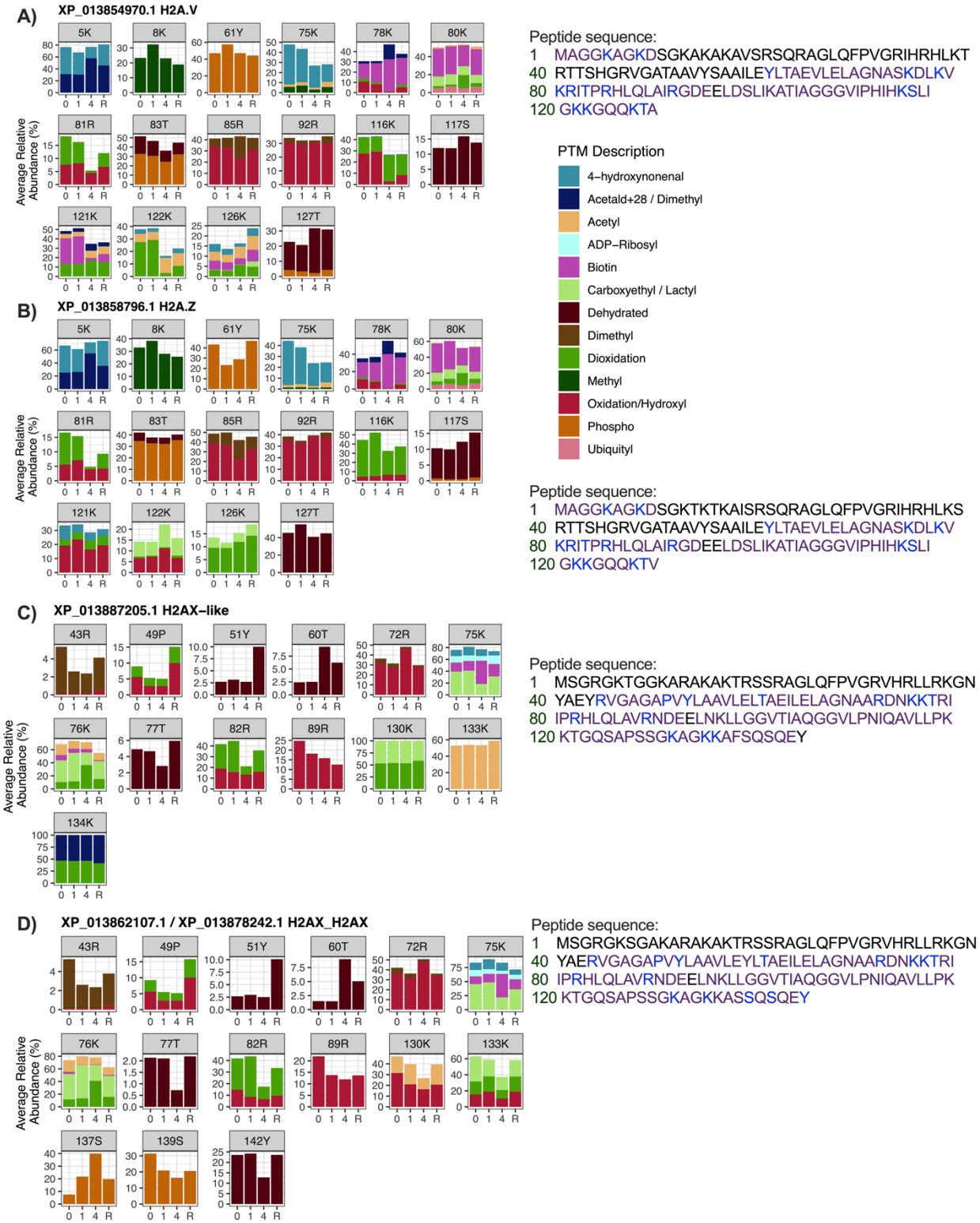

Figure 9. Characterization of the post-translational modifications on histone H2A isoforms in WS40NE cells exposed to anoxia and aerobic recovery from anoxia. (**A**) H2A.V (XP_013854970.1), (**B**) H2A.Z

292 (XP_013858796.1), (**C**) H2AX-like (XP_013887205.1), and (**D**) H2AX-like (XP_013862107.1/ XP_013878242.1).
293 Each panel represents a different amino acid position where at least one hPTM was detected. Amino acid residues
294 are abbreviated using their one letter code. The x-axis displays the condition of the samples: 0 d in anoxia (0), 1 d in
295 anoxia (1), 4 d in anoxia (4), or 1 d of aerobic recovery following 4 d of anoxia (R). The y-axis scales differ across
296 panels to better visualize changes in low abundance hPTMs. Detected (purple) and modified (blue) peptides and the
297 entire peptide sequences are listed beside the panels. On each row, the number of the corresponding residue is listed
298 in green.

299

300 ***Characterization of histone H2B***

301 At least five H2B proteins were identified: (**A**) H2B_1/2-like (XP_013874662.1), (**B**) H2B_1/2
302 (XP_013879561.1 / XP_013878239.1 / XP_013878163.1 / XP_013869445.1), (**C**) H2B_1/2-like
303 (XP_013857090.1), (**D**) H2B.L4-like (XP_013885354.1), and (**E**) H2B.3-like
304 (XP_013886452.1). Thirteen types of PTMs were identified across these isoforms (Fig. 10A).
305 Three hundred and twenty-seven significant hPTMs were present across H2B isoforms in at least
306 one condition, making this the most significantly modified class of histones in this study (Fig.
307 10B). All identified H2B isoforms had at least one residue with a significant hPTM, while 4 of
308 the 5 were highly modified (Fig. 10C). The top three most commonly significant differential
309 hPTMs across H2B isoforms were phosphorylation (58 significant unique hPTMs), dehydration
310 (49 significant unique hPTMs), and oxidation/hydroxylation (35 significant unique hPTMs) (Fig.
311 10A).The following hPTMs displayed an average relative abundance of exactly 100% in all
312 samples: H2B.L4-like (XP_013885354.1) 31Y, 43T, 46S, and 55S dehydration (Fig. 11, Table
313 1).

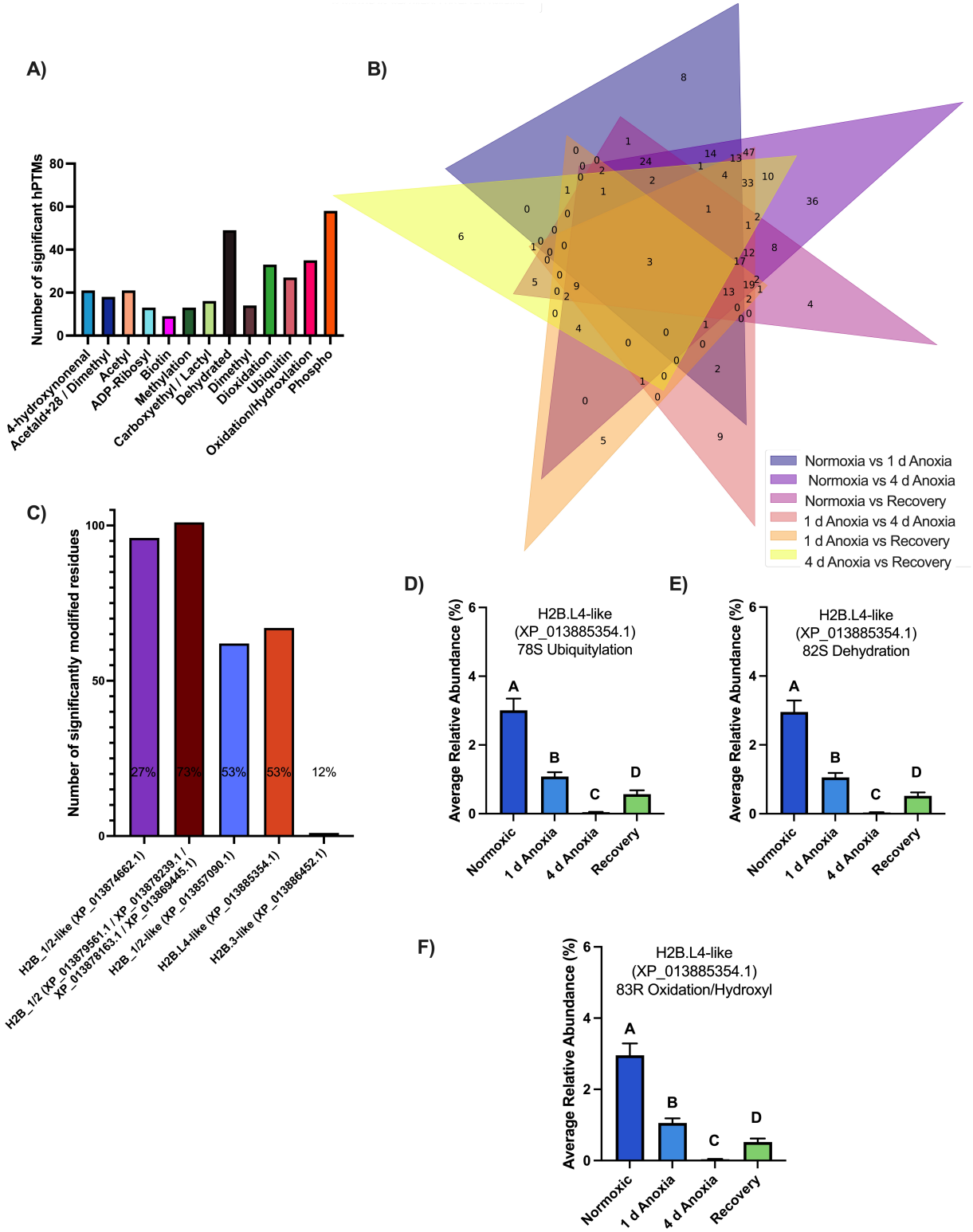

314

315 **Figure 10. Significant differential post-translational modifications on histone H2B isoforms in WS40NE cells**

316 **exposed to anoxia and aerobic recovery from anoxia. (A)** The top three most commonly significant differential

317 hPTMs across H2B isoforms were phosphorylation (58 hPTMs), dehydration (48 hPTMs), and
318 oxidation/hydroxylation (35 hPTMs). (**B**) Venn diagram illustrating the occurrence of unique and biologically-
319 relevant hPTMs on H2B histone isoforms across experimental treatment groups. The Venn diagram is schematic and
320 non-proportional. The numbers within each colored section indicate the number of significantly differentially
321 expressed histone modifications shared among the indicated pairwise comparisons. (**C**) At least five H2B isoforms
322 had residues with significant hPTMs. The percentage above each bar represents the peptide sequence coverage of
323 that isoform. Three hPTMs on H2B.L4-like (XP_013885354.1) were highly condition dependent across all six
324 comparisons: **(D)** 78S ubiquitylation, **(E)** 82S dehydration, and **(F)** 83R oxidation/hydroxylation. Bars represent the
325 mean ± SEM (n=11-12).

326 Three hPTMs on H2B.L4-like (XP_013885354.1) were highly condition dependent across all six
327 comparisons: 78S ubiquitylation, 82S dehydration, and 83R oxidation/hydroxylation (Fig.
328 10D,E,F). An additional twenty-three hPTMs were highly condition dependent across five
329 different comparisons on four different histone isoforms: eight on H2B_1/2-like
330 (XP_013874662.1), seven on H2B_1/2 (XP_013879561.1 / XP_013878239.1 / XP_013878163.1
331 / XP_013869445.1), four on H2B_1/2-like (XP_013857090.1), and four on H2B.L4-like
332 (XP_013885354.1) (Fig. 11, Table 2). Two of these highly condition-dependent modifications on
333 H2B.L4-like (XP_013885354.1) occur on the same residue: 79T dehydration and
334 phosphorylation (Fig. 11D, Table 2).
335

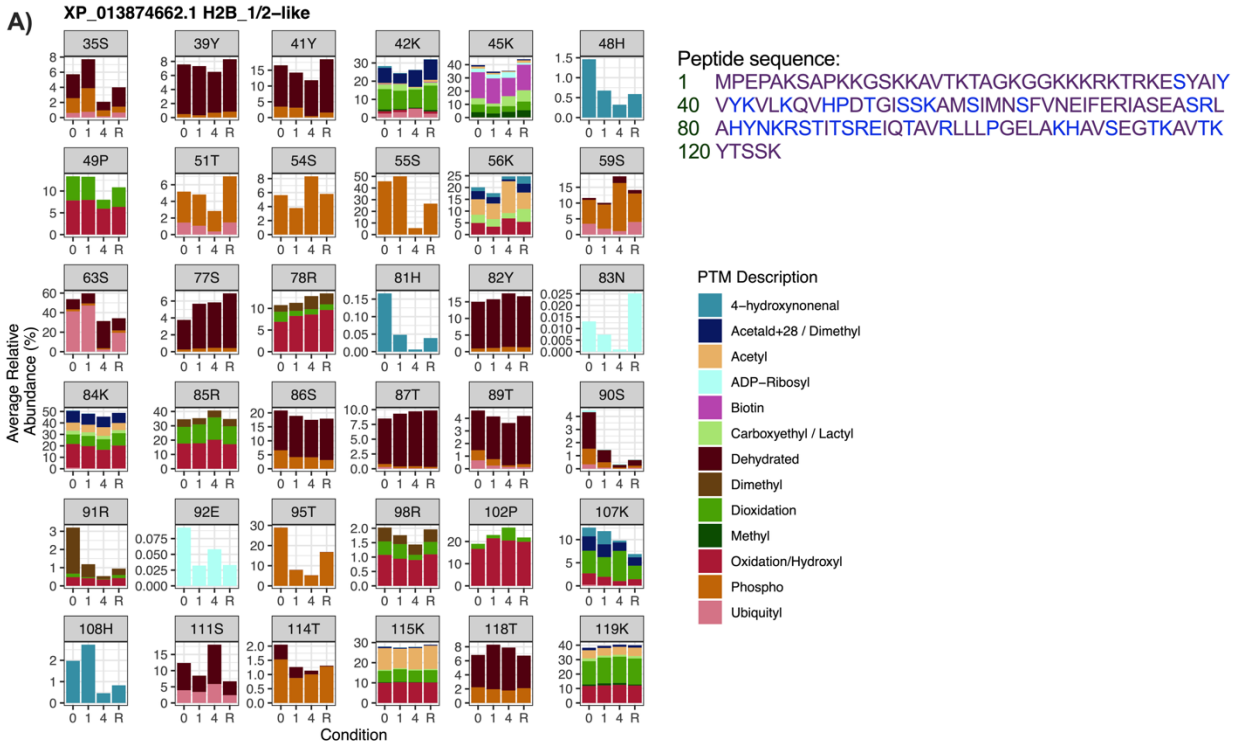
A)
XP_013874662.1 H2B_1/2–like
Peptide sequence:
1 MPEPAKSAPKKGSKKAVTKTAGKGGKKKRKTRKESYAIY
40 VYKVLKQVHPDTGISSKAMSIMNSFVNEIFERIASEASRL
80 AHYNKRSTITSREIQTAVRLLLPGELAKHAVSEGTKAVTK
120 YTSSK
PTM Description
4–hydroxynonenal
Acetald+28 / Dimethyl
Acetyl
ADP–Ribosyl
Biotin
Carboxyethyl / Lactyl
Dehydrated
Dimethyl
Dioxidation
Methyl
Oxidation/Hydroxyl
Phospho
Ubiquityl
Average Relative Abundance (%)
Condition

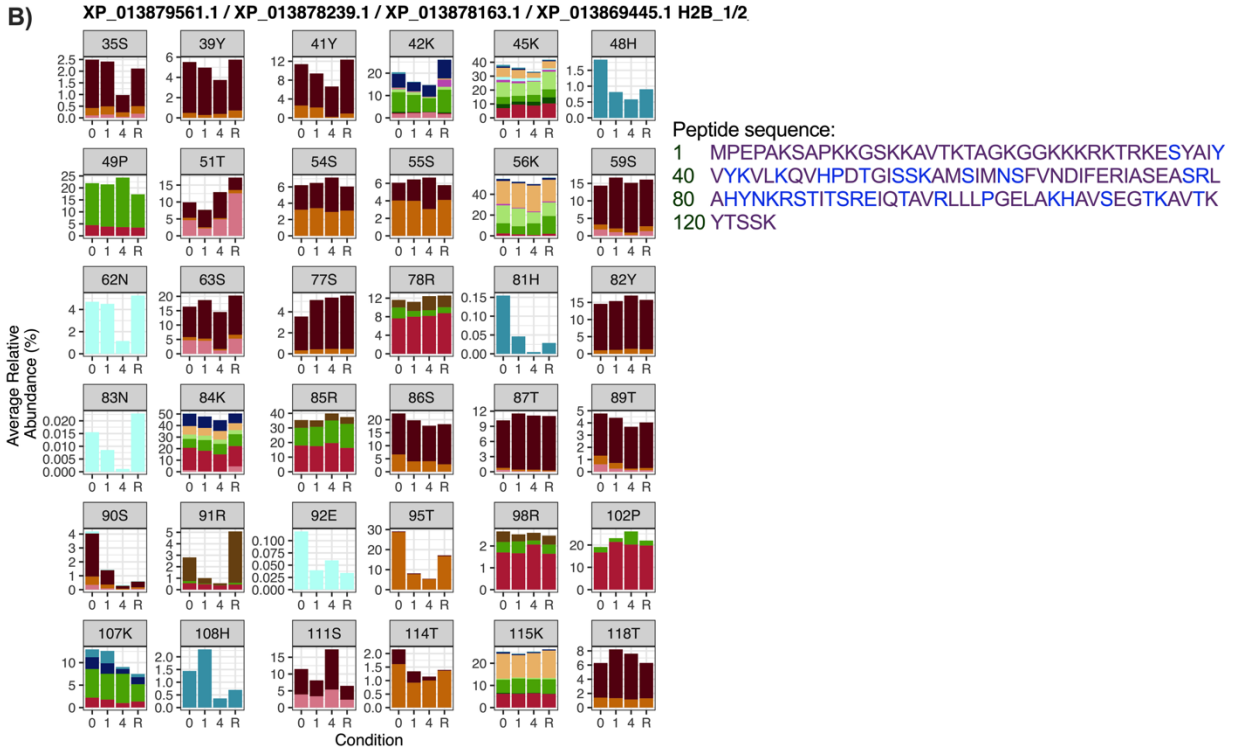
B)
XP_013879561.1 / XP_013878239.1 / XP_013878163.1 / XP_013869445.1 H2B_1/2
Peptide sequence:
1 MPEPAKSAPKKGSKKAVTKTAGKGGKKKRKTRKESYAIY
40 VYKVLKQVHPDTGISSKAMSIMNSFVNDIFERIASEASRL
80 AHYNKRSTITSREIQTAVRLLLPGELAKHAVSEGTKAVTK
120 YTSSK
Average Relative Abundance (%)
Condition

336

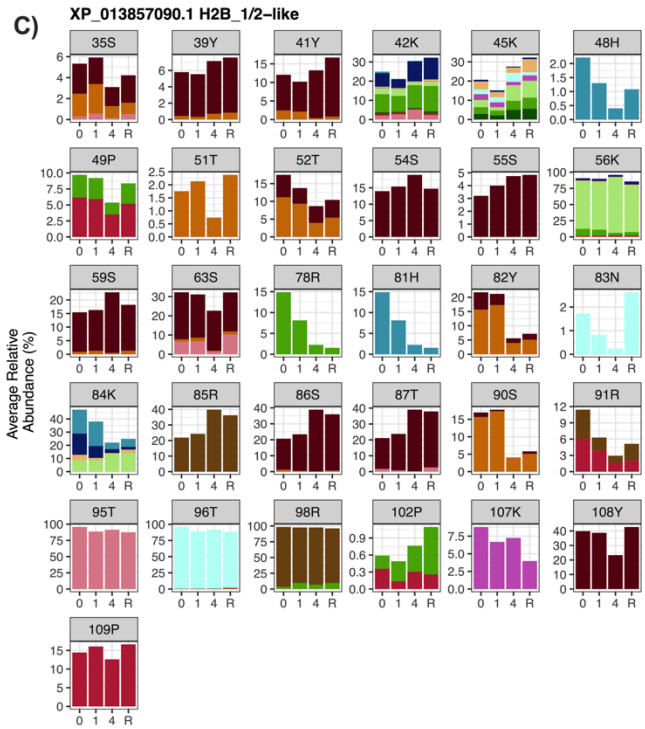

Peptide sequence:
1 MPEPAKSAPKKGSKKAVTKTAGKGGKKKRKTKKESYAIY
40 VYKVLKQVHPDTTISSKAVSFMNSFVNNIFERIASKASRL
80 AHYNKRSTITSREIQTTVRLLLPGELAKYPNN

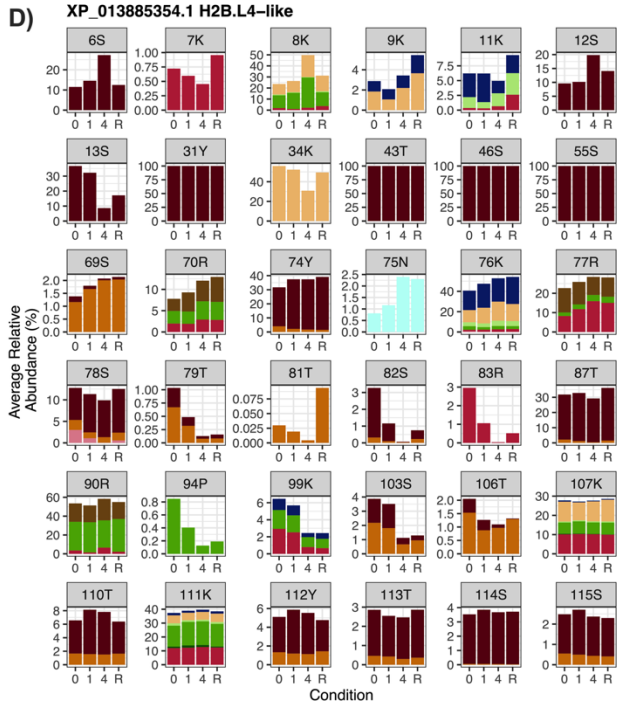

Peptide sequence:
1 MSNDVSKKKGKSSGDKKAKRKVKRRETYAMYIYKVLKQV
40 HPDTGISSRAMSIMNSFVNDLFERIATEASRLAQYNKRST
80 ITSREVQTAVRLLLPGELAKHAVSEGTKAVTKYTSSK

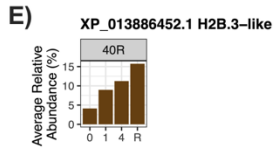

Peptide sequence:
1 MSIMNSFINIFKRIASKASHLAHYCKRSTITSREIQTDV
40 RLLLPGELAKHTMSKGTKAXTKYTSSX

337

338

339 **Figure 11. Characterization of the post-translational modifications on histone H2B isoforms in WS40NE cells**
340 **exposed to anoxia and aerobic recovery from anoxia.** Isoforms represented are (**A**) H2B_1/2-like
341 (XP_013874662.1), (**B**) H2B_1/2 (XP_013879561.1/ XP_013878239.1 / XP_013878163.1 / XP_013869445.1), (**C**)
342 H2B_1/2-like (XP_013857090.1), (**D**) H2B.L4-like (XP_013885354.1) and (**E**) H2B.3-like (XP_013886452.1).
343 Each panel represents a different amino acid position where at least one hPTM was detected. Amino acid residues
344 are abbreviated using their one letter code. The x-axis displays the condition of the samples: 0 d in anoxia (0), 1 d in
345 anoxia (1), 4 d in anoxia (4), or 1 d of aerobic recovery after 4 d of anoxia (R). The y-axis scales differ across panels
346 to better visualize changes in low abundance hPTMs. Detected (purple) and modified (blue) peptides and the entire
347 peptide sequences are listed beside the panels. On each row, the number of the corresponding residue is listed in
348 green.

349 ***Characterization of histone H3***

350 At least three H3 proteins were identified: (**A**) H3.3 (XP_013887037.1 / XP_013885059.1 /
351 XP_013879174.1 / XP_013870443.1), (**B**) H3-like (XP_013879564.1), and (**C**) H3-like
352 (XP_013878241.1). All identified H3 isoforms had at least one residue with a significant hPTM,
353 with 12 types of hPTMs identified across these isoforms (Fig. 12A). The most common hPTMs
354 that differ significantly across experimental treatments on H3 isoforms were
355 oxidation/hydroxylation (23 significant unique hPTMs) and dioxidation (18 significant unique
356 hPTMs) (Fig. 12A). Eighty-nine hPTMs were present across all three H3 isoforms in at least one
357 condition (Fig. 12B). Two hPTMs displayed an average relative abundance of exactly 100% in
358 all samples: H3-like (XP_013878241.1) 17K and 24R oxidation/hydroxylation (Fig. 13C, Table
359 1).

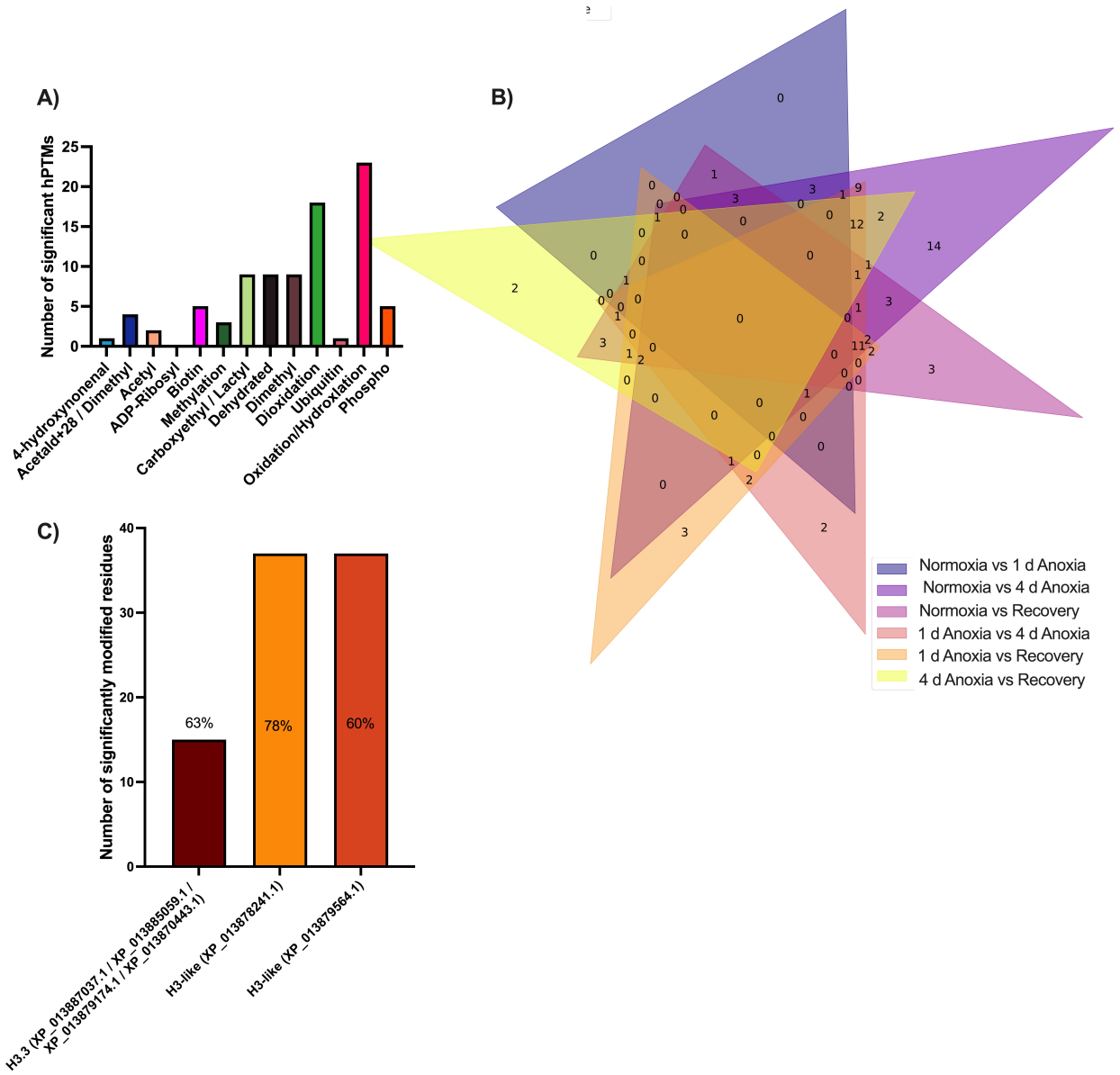

Figure 12. Significant differential post-translational modifications on histone H3 isoforms in WS40NE cells exposed to anoxia and aerobic recovery from anoxia. (A) The most commonly significant differential hPTMs across H3 isoforms were oxidation (23 hPTMs) and dioxidation (18 hPTMs). (**B**) Venn diagram illustrating the occurrence of unique and biologically-relevant hPTMs on H3 histone isoforms across experimental treatment groups. The Venn diagram is schematic and non-proportional. The numbers within each colored section indicate the number of significantly differentially expressed histone modifications shared among the indicated pairwise

367 comparisons. (**C**) All identified H3 isoforms had residues with significant hPTM modifications. The percentage

368 above each bar represents the peptide sequence coverage of that isoform (n=11-12).

369

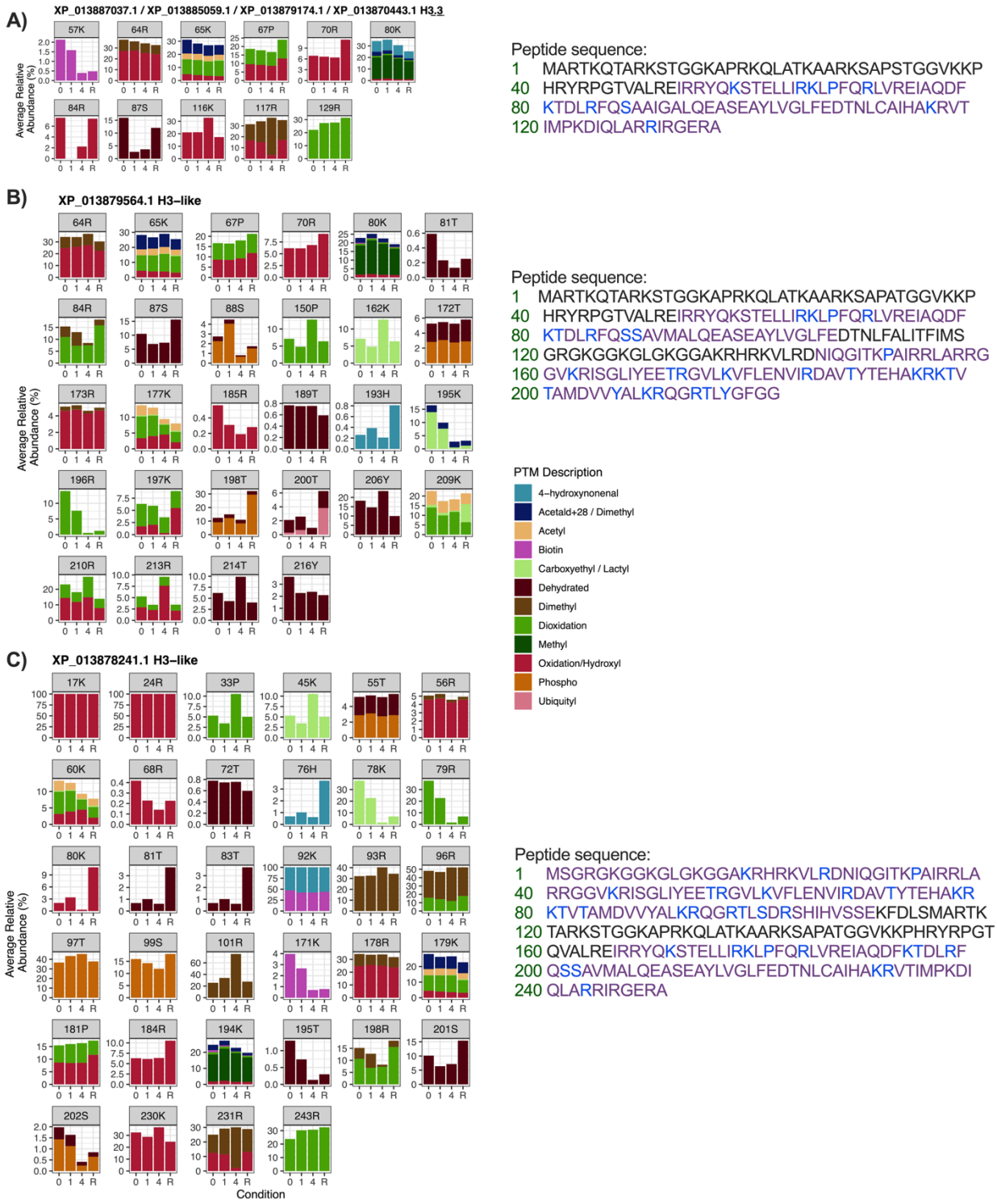

Figure 13. Characterization of the post-translational modifications on histone H3 isoforms in WS40NE cells exposed to anoxia and aerobic recovery from anoxia. Isoforms represented are (**A**) H3.3 (XP_013887037.1/ XP_013885059.1/ XP_013879174.1 / XP_013870443.1), (**B**) H3-like (XP_013879564.1), and (**C**) H3-like

374 (XP_013878241.1). Each panel represents a different amino acid position where at least one hPTM was detected.
375 Amino acid residues are abbreviated using their one letter code. The x-axis displays the condition of the samples: 0
376 d in anoxia (0), 1 d in anoxia (1), 4 d in anoxia (4), or 1 d aerobic recovery after 4 d of anoxia (R). The y-axis scales
377 differ across panels to better visualize changes in low abundance hPTMs. Detected (purple) and modified (blue)
378 peptides and the entire peptide sequences are listed beside the panels. On each row, the number of the corresponding
379 residue is listed in green.

380

381

382 ***Extracellular Lactate Accumulation***

383 While previous studies have explored accumulation of lactate during exposure to anoxia in
384 WS40NE cells, this was the first study to monitor how this lactate accumulation persisted during
385 recovery (Fig. 14). As previously shown, anoxic WS40NE cells accumulate extracellular lactate
386 at a significantly higher rate than normoxic cells. After 1 d of aerobic recovery, this trend
387 persists.

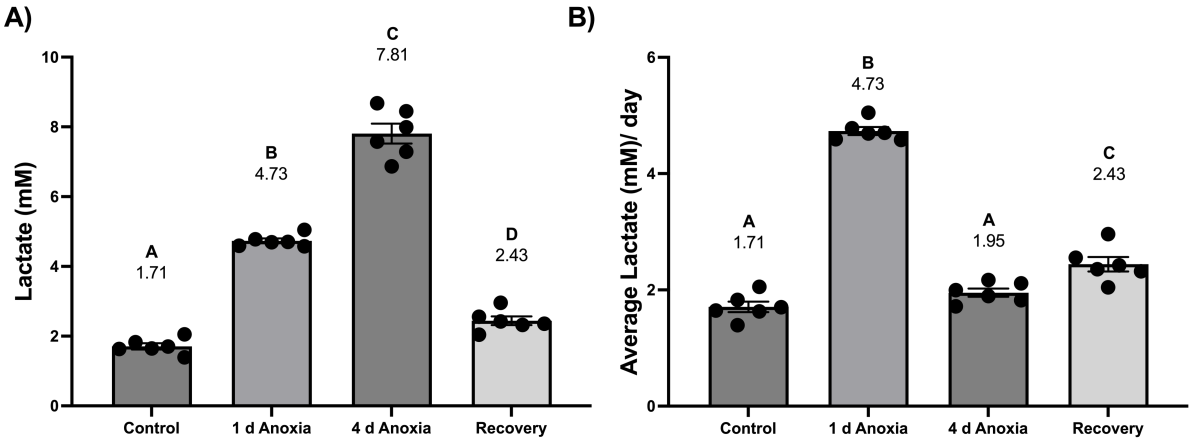

388

389 **Figure 14. Extracellular lactate accumulation in WS40NE cells exposed to anoxia and recovery from anoxia.**
390 (**A**) Total media lactate concentration (mM) during exposure to anoxia and recovery from anoxia. Due to the
391 recovery media change, the data represents only 1 day of lactate accumulation in normoxic recovery conditions. (**B**)
392 The average rate of lactate accumulation (mM/day) in the same samples. Different letters indicate significant
393 differences in means within each graph (one-way ANOVA with Tukey's HSD test $p > 0.05$, $n = 6$).

394 **Discussion**

395 Histone isoforms and post-translational modifications change in response to anoxia and aerobic
396 recovery from anoxia in WS40NE cells. Of the 1043 unique biologically relevant hPTMs
397 detected, 816 hPTMs were significantly modified in at least one condition. All identifiable
398 histone groups showed significant post-translational modifications in response to changing

399 oxygen availability. H2B was the most significantly modified histone group with 327 significant
400 differential hPTMs present in at least one condition. H2B_1/2 (XP_013879561.1 /
401 XP_013878239.1 / XP_013878163.1 / XP_013869445.1) was the most significantly modified
402 histone, with 101 significant modifications. Interestingly, highly condition-dependent hPTMs
403 often occurred on adjacent residues, with two highly condition-dependent hPTMs sharing a
404 single residue. This suggests that histones of WS40NE cells have highly modifiable peptide
405 regions that are responsive to changes in oxygen availability and likely help to coordinate
406 changes in gene expression associated with their extreme anoxia tolerance. In many aspects, this
407 response is consistent with hypoxic responses in hPTMs observed in human cells [39, 40],
408 including several stress related hPTMs, such as oxidation/hydroxylation and dioxidation,
409 increasing globally in response to anoxic stress and aerobic recovery due to increased rates of
410 reactive oxygen species (ROS) production [41, 42]. However, WS40NE cells demonstrate
411 several unexpected responses to changing aerobic conditions, including changes in histone
412 isoform abundance and several unique trends in hPTMs.

413 ***Limitations and precautions in the interpretation of these data***

414 One limitation of this study is the lack of detection of histone H4. This result is consistent with
415 previous studies using these methods in *A. limnaeus* [34] and in other fish species [20, 43]. As
416 previously discussed, this is likely due to the specific nature of the single histone H4 sequence in
417 *A. limnaeus* and the limited number of potential ions available for detection using these
418 methodologies. In addition, it is important to note that while there is a great deal of sequence
419 conservation for histone across species, some sequences in *A. limnaeus* contain long N-terminal
420 tails that make direct comparisons of the "classic" histone modifications difficult (see discussion
421 in [34]). It also means that for those isoforms, what is considered a "tail" in a mammalian protein

422 becomes more central in *A. limnaeus*, despite the tail portion of the protein being highly
423 modified (e.g. Figure 13c). The significance of these differences is unknown but should be
424 considered when comparing these data to those in other species.
425
426 ***Changes in histone isoform abundance***
427 Several histone isoforms change in abundance in response to anoxia. While, to our knowledge,
428 no study has identified anoxia-dependent changes in histone isoform abundance, there are
429 several studies that document changes in histone isoforms in response to heat stress, hypoxia,
430 ischemia, and oxidative stress [40, 44-46]. Notably, one of the histone variants to show
431 significant changes in abundance in our study H3.3, is generally deposited via histone cell cycle
432 regulator (HIRA) in a replication-independent manner [40, 47], suggesting that its hPTM and
433 isoform abundance changes are not due to the cell division that can occur during anoxia [37].
434 The increase in histone H3.3 observed in this study is consistent with a role for "priming" the
435 cells for a robust gene expression response to stress as has been shown in human lung fibroblasts
436 [40]. Importantly, histone H3.3 expression responds within 1 day of anoxia and does not
437 immediately return to pre-anoxic levels after 1 day of recovery, suggesting a prolonged change
438 in poise of the chromatin. H3.3 is typically associated with euchromatin and active regulatory
439 elements [48], suggesting that the genomic location of the histone H3.3 isoforms may indicate
440 genes that are immediately responsible for supporting cellular functions in the absence of
441 oxygen, or may represent genes primed and ready to be expressed during recovery from anoxia.
442 If future studies can identify the genomic location of the H3.3 isoforms, these genes would be
443 prime candidates for explaining anoxic-preconditioning in embryos of *A. limnaeus* [49].
444

445 The other differentially abundant isoforms are most closely related to canonical H2A and H2B
446 isoforms [50], which can be exchanged via replication dependent mechanisms [51]. However,
447 these isoforms can also be exchanged via replication independent mechanisms including
448 complexes formed by histone chaperone nucleosome assembly protein 1 (NAP-1) or facilitates
449 chromatin transcription (FACT) protein [52-54]. Given that FACT can be recruited during
450 hypoxia to modulate both histone ubiquitylation and transcriptional activation of hypoxia-
451 induced genes, the ability of these complexes to exchange histone isoforms could very well also
452 be a part of the anoxic stress response [55]. H2A/H2B dimers flank entry and exit portals for
453 DNA in the nucleosome, and thus changes to these histone isoforms are highly likely to impact
454 gene expression [51, 56]. In WS40NE cells, one histone H2A isoform decreases within 1 day of
455 anoxia, while two histone H2B isoforms decrease, but only after 4 days of anoxia, suggesting
456 unique regulation and usage of these isoforms in response to anoxia. Histone H2A isoforms have
457 been shown to increase after exposure to hypoxia and ischemia in some mammalian models [57,
458 58], a result that is opposite of that in WS40NE cells. The reason for this shift and their potential
459 for altering gene expression is worthy of future studies.

460 ***Global decreases in multiple hPTMs deviate from expected patterns***

461 Global changes to hPTMs have been recorded in mammalian cells in response to hypoxia; large
462 changes in modifications of H3 and H4 histones are seen in HEK 293T, HeLa and RKO cells
463 with smaller changes occurring on H2A and H2B histones [39]. However, few studies have
464 investigated anoxia-induced changes in hPTMs in a modification-specific way [34].
465 Interestingly, global methylation in WS40NE cells is stable for the first day of anoxia, but then
466 significantly decreases during 4 d anoxia and remains low for 1 d of aerobic recovery. As
467 H3K4me3 and H3K36me3 increase within 1 h during hypoxia in mammalian systems, we

468 expected global methylation in *A. limnaeus* to reflect similar changes [28]. Increases in
469 methylation in hypoxic mammalian systems is thought to be due to decreased activity of histone
470 demethylases when oxygen is limiting, mainly because many of these enzymes use molecular
471 oxygen as a substrate, and at least one histone demethylase appears to be upregulated in a
472 hypoxia-inducible factor dependent manner, presumably to combat the overall loss of
473 demethylase activity during hypoxia [59]. Thus, the large and sustained decrease in global
474 methylation exhibited in killifish WS40NE cells is an unexpected result when referenced to the
475 mammalian literature. Histone methylation, including di- and trimethylation, is associated with
476 transcriptional activation and repression in a residue specific manner [60, 61], so it is difficult at
477 this time to draw any conclusions for the role that decreased methylation might play. Of note,
478 only one site of methylation in our dataset was highly condition dependent (H2B_1/2,
479 XP_013874662.1 and XP_013869445.1, 124K). This residue does not correspond with any
480 known mammalian hPTMs but may serve a similar function and should be investigated further.

481 Given its role in the regulation of DNA repair [62], it is surprising that global levels of ADP-
482 ribosylation consistently decrease in anoxia and remain depressed during aerobic recovery. Most
483 residue-specific patterns match this global pattern with either stable or decreasing levels of ADP-
484 ribosylation during anoxia. However, in the cases where an increase occurs on a specific residue,
485 it is almost always during aerobic recovery. This suggests a conserved role for ADP-ribosylation
486 of histones associated with oxidative stress and the DNA damage response [62, 63]. However,
487 PARPs including diphtheria-toxin-like ADP-ribose transferases (ARTDs) and cholera-toxin-like
488 ARTCs can modify a variety of residues: lysine, aspartate, glutamate, serine, arginine, tyrosine,
489 and histidine [64, 65]. Additionally, ADP-ribosylation can occur on arginine, serine, threonine,
490 and cysteine residues via the action of sirtuins (SIRT4, SIRT6, and SIRT7) that perform mono

491 (ADP-ribose) (MAR) addition [64]. Histone ADP-ribosylation is associated with a variety of
492 functions beyond DNA damage response, including chromatin remodeling and facilitation of
493 gene transcription by making chromatin more accessible [66, 67]. A decrease in ADP-
494 ribosylation may be associated with a decrease in chromatin availability, decreasing the
495 accessibility of the genome to polymerases and transcription factors. Thus, the overall decrease
496 in histone ADP-ribosylation may support the downregulation of transcription associated with
497 entrance into anoxia-induced quiescence.

498 Recent studies suggest lactate accumulation in mammalian cells may play a role in cell signaling
499 and regulation through histone lactylation [68], including stimulating gene transcription in
500 macrophages [69]. WS40NE cells accumulate extracellular lactate throughout anoxia and during
501 at least the first day of aerobic recovery. Lactate is a glycolytic end-product that has classically
502 been considered an unavoidable consequence of vertebrate anaerobic metabolism, but in
503 WS40NE cells, 49 of 70 total unique carboxyethylation/lactylation modifications significantly
504 changed in abundance in at least one comparison and one of these modifications was classified
505 as highly condition dependent (Table 2). Given the extreme rarity of protein carboxyethylation,
506 these modifications are most likely sites of lactylation [70]. Surprisingly, increased lactate
507 accumulation in WS40NE cells is correlated with *decreased*, not increased, global
508 carboxyethylation/lactylation. This pattern is the opposite of what is seen in human MCF-7,
509 HeLa, and MDA-MB-231 cells, which exhibit a dose-dependent increase in histone lactylation in
510 response to 25 mM exogenous L-lactate [69]. Further, in almost all cases, residues in WS40NE
511 histones experience a decrease in lactylation during anoxia. It is possible that the slower rate of
512 lactate accumulation in WS40NE cells (7.8 mM extracellular lactate after 4 days of anoxia) does
513 not produce enough lactate to cause increase lactylation. However, lactate levels are relatively

514 low during normoxia, and yet many histone residues still have a high percentage of lactylation.
515 Thus, lactate availability is not likely to limit histone lactylation in WS40NE cells. It is worth
516 considering that decreased rates of lactate accumulation and decreased histone lactylation in
517 WS40NE cells may at least partially underlie their extreme anoxia tolerance, as this is contrary to
518 trends that appear in anoxia intolerant mammalian cells.

519 ***Dehydration and phosphorylation – a reciprocal relationship?***

520 Dehydration of residues in WS40NE cell histones increases globally, while conversely, global
521 phosphorylation decreases during anoxia and aerobic recovery from anoxia. These patterns are
522 surprising, and the apparent reciprocal patterns of abundance are potentially very interesting.

523 One important site of phosphorylation was detected in WS40NE histones: H2A.X 137S.
524 Phosphorylation of mammalian 139S (γ–H2A.X) initiates the DNA repair response and would
525 therefore be expected to increase during anoxia due to an increase in ROS-induced DNA damage
526 [71]. Surprisingly, 137S, the equivalent residue in WS40NE histone H2A.X, experiences a
527 decrease in phosphorylation by 1 day in anoxia and continues to decrease during 4 days of
528 anoxia. Interestingly, a nearby dehydrated residue, 142Y, follows the opposite pattern, increasing
529 during anoxia. In this dataset, phosphorylation never occurs at this tyrosine residue. This is
530 unexpected, as constitutive phosphorylation of mammalian 142Y by Williams–Beuren syndrome
531 transcription factor (WSTF) occurs during normal conditions while dephosphorylation of this
532 site occurs during the DNA damage response [72]. This dephosphorylation has been theorized to
533 enhance recruitment of protein kinases to better maintain γ–H2A.X phosphorylation [72].
534 Therefore, it is interesting that this site is dehydrated, as dehydration may prevent
535 phosphorylation and thus prevent the dampening of the DNA damage response that is observed

536 in mammalian cells [72]. These sites should be explored in the future, as they are implicated in
537 regulation of transcription and DNA replication may have nearby sites of dehydration that are
538 involved in their modification status [73].

539 ***Multiple hPTMs do not return to baseline after 1 day aerobic recovery***

540 The histone landscape of WS40NE cells remains altered after 1 day of aerobic recovery from 4
541 days of anoxia. It is important to note that for these cells, 4 days is a relatively short duration of
542 anoxia given they can survive for 49 days without oxygen [37]. Globally, 8 of the 13 types of
543 hPTMs detected are significantly different in recovery compared to normoxia. Based on the $\log_2$
544 fold-change, global acetylation, oxidation/hydroxylation, and dioxidation are significantly
545 elevated during recovery while global phosphorylation, biotinylation, 4-hydroxynonenal,
546 methylation, and carboxyethylation/lactylation are all decreased. Of the unique hPTMs that were
547 significantly modified, 42% are associated with recovery. While many of the hPTMs may simply
548 not have returned to baseline, other modifications may be involved in recovery mechanisms.
549 Further work will need to be done to determine if these hPTMs return to normoxic levels, or if
550 they represent potential heritable epigenetic alterations to the histone landscape and act as a
551 cellular memory of past exposures to anoxia.

552 **Conclusion**

553 WS40NE cells are unique in their ability to survive long bouts of anoxia and demonstrate
554 changes in their histone landscape in response to different lengths of time in anoxia and recovery
555 from anoxia. This response includes altering both histone isoform relative abundance and hPTM
556 relative abundance at multiple amino acid positions. This response likely contributes to the
557 anoxia tolerance displayed in this cell type. Downstream effects of specific hPTM changes

558 should be studied in the future to determine how specific hPTMs can impact gene expression and
559 anoxia tolerance. Of specific interest is the potential reciprocal relationship between dehydration
560 and phosphorylation as a regulatory mechanism to alter gene expression in response to anoxia.
561

562 **Methods**

563 ***WS40NE Cell Maintenance and Anoxic Exposure***

564 Cells were grown in cell culture media (L-15 + 8.5% FBS, 5 mM glucose, 100 U/mL penicillin/
565 streptomycin) in 100 × 20 mm tissue culture dishes at 30°C and split when confluent using
566 TrypLE Express [37]. For all anoxic experiments, plates of cells were seeded at 2.5 x 10^6 cells
567 per plate and given 24 h to adhere. Cells were then introduced into an anoxic chamber (Bactron
568 EZ, Sheldon Manufacturing, Cornelius, OR, USA) that contains an atmosphere of 95% N_2 and
569 5% H_2. Media was immediately replaced with anoxic media that had been purged with N_2 gas for
570 30 min and then pre-equilibrated to the atmosphere of the anoxic chamber overnight. Cells were
571 harvested at **A)** 0 h of anoxia (normoxic), **B)** 1 d of anoxia, **C)** 4 d of anoxia, and **D)** after 1 d of
572 aerobic recovery following 4 d of anoxia (n = 12). To harvest, media was removed and a cell
573 scraper was used to gently dissociate cells from the bottom of the plate. Two 100 × 20 mm tissue
574 culture dishes were pooled for each replicate. Cell pellets were generated by subjecting the
575 isolated cells to centrifugation at 500 x *g* for 7 min at 4° C, and removing the supernatant.
576 Additionally, media samples were taken directly prior to the harvest of all four timepoints and
577 used to determine the levels of extracellular lactate accumulation. Cell pellets and spent media
578 were flash frozen in liquid nitrogen. Samples were stored at -80° C until use for histone acid
579 extraction or determination of lactate concentration.

580 ***Histone Acid Extraction and Protein Digestion***

581 A middle-down approach to proteomics was used for liquid chromatography mass spectrometry
582 (LCMS) using previously described methods [34, 43]. This workflow was chosen due to its
583 previous success in capturing histone peptide fragments in tissue of adult Mozambique tilapia
584 (*Oreochromis mossambicus*) and *A. limnaeus* embryos [34, 43]. Histone acid extracts were
585 generated by resuspending cell pellets in 0.4 N H_2SO_4 and incubating the samples with constant
586 rotation at 4 °C for 4 h. Samples were then centrifuged at 16,000 x *g* for 10 min at 4 °C and the
587 supernatant was transferred into a fresh 1.5 mL tube. This process was repeated twice.
588 Trichloroacetic acid (TCA) was added to each sample drop-by-drop until a volume equal to 25%
589 of the estimated sample volume had been added. Samples were inverted to mix and incubated
590 overnight at 4 °C. Once the histone proteins had precipitated, samples were centrifuged at 3,400
591 x *g* for 5 min at 4 °C, and the supernatant was discarded. The remaining pellet was rinsed twice:
592 first in ice cold acetone with 0.1% hydrochloric acid and then with 100% acetone. For both
593 rinses, the samples were centrifuged at 3,400 x *g* for 2 min at 4 °C and the supernatant was
594 removed. After both rinses were complete, histone pellets were air dried in a fume hood for 5
595 min. Samples were stored at -80 °C until the in-solution digestion.
596
597 To begin the digestion, each sample was brought to room temperature (RT), and the histone
598 pellet was resuspended in 138 μL of 8 M urea. Dithiothreitol (DTT) was added to a final
599 concentration of 10 mM. Each sample was then briefly vortexed, centrifuged, and incubated at
600 37 °C for 30 min. Iodoacetamide (IAA) was added to each sample to a final concentration of 30
601 mM, and samples were briefly vortexed and centrifuged before a 30 min incubation in the dark at
602 RT. Samples were briefly vortexed and centrifuged again after the incubation and protein

603 concentration was determined through a bicinchoninic acid (BCA) assay, (cat# 23250, Thermo
604 Scientific, Waltham, MA, USA). Each sample (50 µg of total protein) was diluted 5:6 (v:v) in
605 0.1M sodium phosphate buffer (pH 7.8). V8 protease beads (cat#20151, Thermo Scientific,
606 Waltham, MA, USA) were added at 1:50 ratio (protease:total protein). In sodium phosphate
607 buffer, V8 protease cleaves proteins at the carboxyl end of both glutamate and aspartate residues.
608 After a 20 h incubation with constant rotation at 30 °C, protease beads were removed by
609 centrifugation at 500 x *g* for 2 min and the supernatants were retained. Supernatants were
610 subjected to an additional centrifugation at 19,000 x *g* for 5 min, and those subsequent
611 supernatants were transferred to fresh tubes and dried using a SpeedVac (Thermo Savant,
612 model# ISS110, Thermo Scientific, Waltham, MA, USA). The peptide pellets were reconstituted
613 to a final concentration of 333 ng/µL in 0.1% formic acid diluted in LCMS-grade water. For
614 peptide clean-up, Pierce C18 Spin Columns (cat# 89873, Thermo Scientific, Waltham, MA,
615 USA) were used according to the manufacturer's instructions.
616
617 Data-dependent acquisition (DDA) was used to generate peak lists [74], and PEAKS Suite X
618 Plus and MSFragger were used to annotate histone peptides using the *A. limnaeus* reference
619 proteome [75]. Utilizing the spectral library that was generated from the DDA run, data-
620 independent acquisition (DIA) was then used to quantify the peptides in the samples using
621 fragment ion–based extraction. A fixed isolation window DIA scheme was applied, with
622 consecutive 10 m/z windows overlapping by 0.5 m/z. The full MS/MS acquisition range spanned
623 *m/z* 370–1090 and collision energy was optimized to specifically match each isolation window.
624 For each peptide, at least four transition peaks were required to be included in the dataset [43,

625 74]. PTMs were assigned by PEAKSPTM software using a minimum localization score of 5%
626 and a minimum Ascore of 20. All data were normalized in Skyline using overall sample median.

627 ***Histone and hPTM Library Generation***

628 Peptides modified with hPTMs were distinguished from unmodified sequences based on their
629 mass shift (Fig. S1). A list of histone PTMs was compiled according to the histone protein name,
630 amino acid residue/position, and modification type using Python code as previously described
631 [34]. All histone PTMs detected were evaluated for their biological relevance (classified as post-
632 translational, other, or multiple) according to their Unimod accession and amino acid residue.
633 Modifications classified by Unimod as known artefacts or chemical derivatives were removed
634 from analysis. Modifications with the same mass shift are listed together. Peptides that mapped
635 to multiple histones in the *A. limnaeus* genome are presented as a protein family and are reported
636 together.

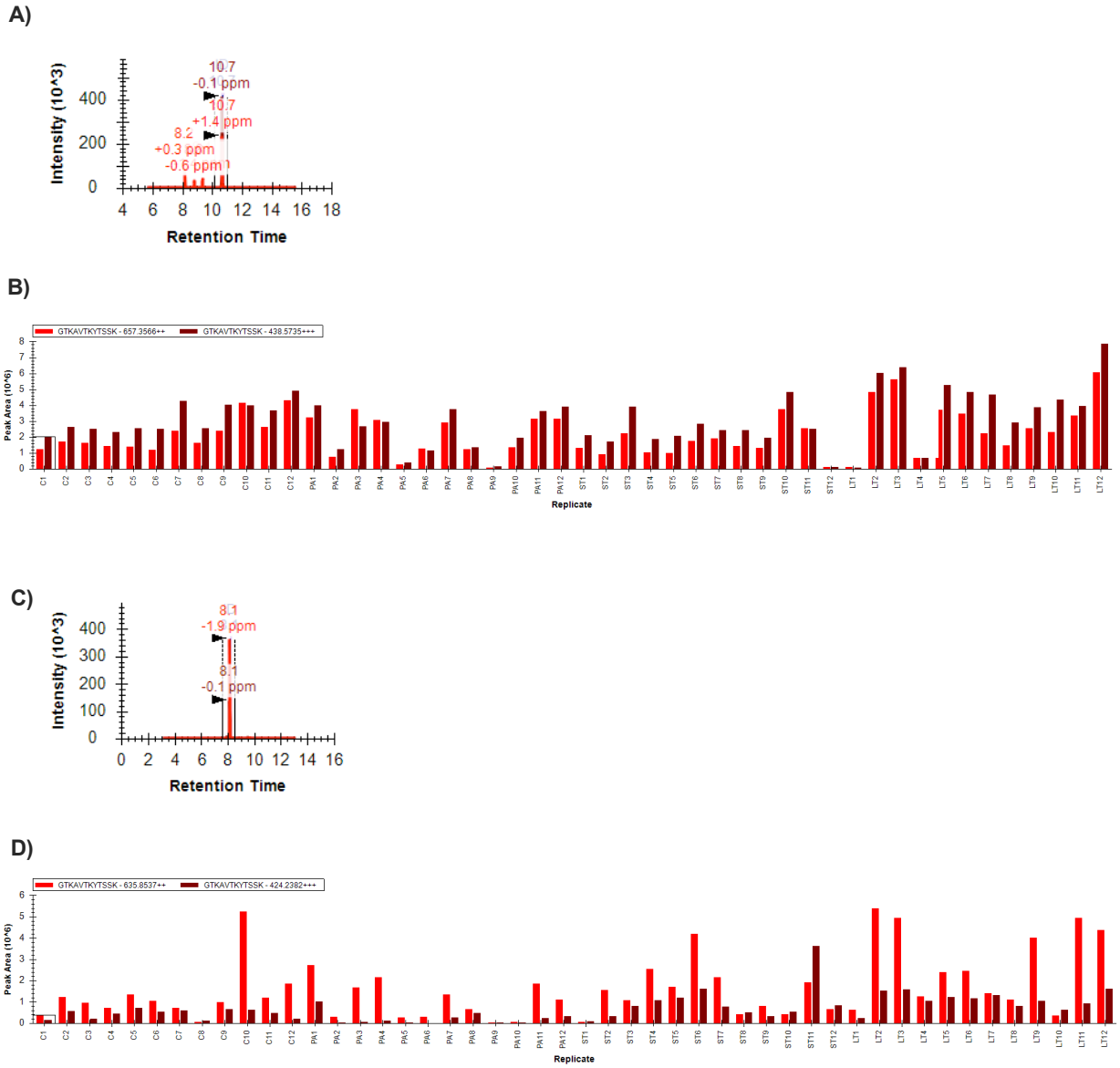

Figure S1: Quantification of histone post-translational modifications in Skyline. A representative MS spectrum (**A**) and peak area (**B**) of the most abundant ions for a modified peptide, E.GTK[+42]AVTKYTSSK, and **(C,D)** the corresponding unmodified peptide E.GTKAVTKYTSSK. Both peptides correspond to histone H2B.L4-like (XP_013885354.1). A mass shift of +42 on a peptide represents acetylation.

Protein Abundance and hPTM Statistical Analyses

643 Histone isoform abundance was evaluated using quantile normalized raw protein abundance data
644 in Python as previously described [34]. Principal component analysis (PCA) and two-tailed t-
645 tests with the Benjamini-Hochberg correction applied to account for multiple hypothesis testing
646 [76] were used to make inferences about histone isoform abundance.

647 Peptide abundance, as determined by normalized area under the curve, and raw protein
648 abundance were obtained using Skyline (Version 22.2) [77]. Relative abundance values (the
649 percent that a specific amino acid residue on a histone is modified by a specific PTM) were used
650 to calculate beta-values and M-values. Beta-value is a transformation of relative abundance
651 expressed as a number between 0 and 1 calculated by adding a value of 100 to the denominator
652 to standardize low intensity peptides [78]. The M-value is a logit transformation of the beta-
653 value [79]. Additionally, the relative abundance of each hPTM was used to calculate the $\log_2$
654 fold change, and a two-tailed t-test was used to compare the relative abundance of hPTMs in all
655 conditions with the Benjamini-Hochberg correction applied to account for multiple hypothesis
656 testing [76]. This relative abundance analysis was repeated to analyze global hPTM levels and
657 calculate the $\log_2$ fold change. Additionally, an ANOVA was performed on the global relative
658 abundance of each hPTM using Prism (ver 10.0.0, GraphPad, Software, Boston, MA, USA). A
659 Dunnett's multiple comparison test was used to determine significance of all conditions
660 compared to normoxia. The global relative coverage of each modifiable amino acid residue was
661 calculated to determine what percentage of each hPTM was present at each modifiable residue.

662 Histone PTM maps were constructed for anoxic and normoxic samples using the mean relative
663 abundance of hPTMs. The M-value was used to perform a principal component analysis (PCA).
664 All abundance plots and PCA plots were made in R using the package ggplot2 [80]. Global
665 hPTM abundance, protein relative abundance, and global relative residue coverage were

666 visualized using Prism (ver 10.0.0, GraphPad, Software, Boston, MA, USA). All Python and R
667 code is accessible by the public on GitHub at
668 https://github.com/hughcj11/WS40NE_Histone_PTM_Analysis. Supplementary data including
669 average relative abundance, t-statistic, p-value, and corrected p-value is provided for each
670 unique, biologically relevant hPTM are provided in Supplementary Table S1 (Excel workbook)
671 across all aerobic conditions.

672 ***Lactate Accumulation Assay***

673 Lactate concentration in the cell culture media was measured enzymatically as previously
674 described [37]. Briefly, each well of a 96-well plate (black walls, clear bottom, Greiner Bio-One,
675 Monroe, NC, USA) contained the following enzyme assay cocktail: 218 µL of Glycine (0.6 M)-
676 Hydrazine (0.5 M) buffer (pH = 9.2), 25 µL 27 mM NAD^+ , 5 µL of lactate standard or sample,
677 and 2.5 µL lactate dehydrogenase (LDH, 14 U/mL, Sigma Aldrich). Change in absorbance was
678 measured at 340 nm every min for 60 min using a plate reader (Tecan Infinity M200Pro,
679 Männendorf, Switzerland). Final concentration of lactate in the samples was determined by
680 interpolation using a lactate standard curve.

681 **Author Contributions**

682 JEP and CH conceived and designed the study. CH and EAM performed the experiments and
683 acquired the data. CH analyzed the data. DK and JEP contributed reagents/materials/analysis
684 tools. CH and JEP wrote the paper. All authors edited and approved the manuscript.
685

686 **Acknowledgements**

We would like to thank Karim Soliman for his guidance in the creation of the Python data analysis pipeline and visualization of the data. We would like to thank Dr. Daniel Zajic for his help performing the lactate accumulation assay.

Funding

Funded by National Science Foundation Grant IOS-2209383 and IOS-2025832.

Data and resource availability

The datasets (DDA and DIA raw data) supporting the conclusions of this article are available in Panorama Public (https://panoramaweb.org/CH0001JP.url) and ProteomeXchange (PXD067707: https://proteomecentral.proteomexchange.org/cgi/GetDataset?ID=PXD067707).

Reviewer login:

Email: panorama+reviewer361@proteinms.net

Password: 3dqk$TMm1AJbo%

703 **References**

704

705 1. Lipton P. Ischemic cell death in brain neurons. Physiological Reviews. 1999;79(4):1431-
706 568.
707 2. Katchanov J, Harms C, Gertz K, Hauck L, Waeber C, Hirt L, et al. Mild cerebral
708 ischemia induces loss of cyclin-dependent kinase inhibitors and activation of cell cycle
709 machinery before delayed neuronal cell death. The Journal of Neuroscience. 2001;21(14):5045-
710 53.
711 3. Andersson BS, Aw TY, Jones DP. Mitochondrial transmembrane potential and pH
712 gradient during anoxia. American Journal of Physiology - Cell Physiology. 1987;252(4):C349-
713 C55.
714 4. Pamenter ME, Gomez CR, Richards JG, Milsom WK. Mitochondrial responses to
715 prolonged anoxia in brain of red-eared slider turtles. Biology Letters. 2016;12(1):20150797. doi:
716 10.1098/rsbl.2015.0797. PubMed PMID: 26763217; PubMed Central PMCID:
717 PMCPMC4785919.
718 5. Galli GLJ, Richards JG. Mitochondria from anoxia-tolerant animals reveals commons
719 strategies to survive without oxygen. J Comp Physiol B. 2014;184:285-302. doi:
720 10.1007/s00360-014-0806-3.
721 6. Hammerman C, Kaplan M. Ischemia and reperfusion injury. The ultimate
722 pathophysiologic paradox. Clin Perinatol. 1998;25(3):757-77. doi: 10.1016/S0095-
723 5108(18)30110-6. PubMed PMID: 9779346.
724 7. Salas-Vidal E, Méndez-Cruz FJ, Ramírez-Corona A, Reza-Medina B. Oxygen, reactive
725 oxygen species and developmental redox networks: Evo-Devo Evil-Devils? The International
726 Journal of Developmental Biology. 2021;65(4-5-6):345-56. doi: 10.1387/ijdb.200170es.
727 8. Scherz-Shouval R, Elazar Z. ROS, mitochondria and the regulation of autophagy. Trends
728 in Cell Biology. 2007;17(9):422-7.
729 9. Kirino T. Delayed neuronal death in the gerbil hippocampus following ischemia. Brain
730 Research. 1982;239(1):57-69.
731 10. Cao W, Carney J, Duchon A, Floyd R, Chevion M. Oxygen free radical involvement in
732 ischemia and reperfusion injury to brain. Neuroscience Letters. 1988;88(2):233-8.
733 11. Feder ME, Hofmann GE. Heat-shock proteins, molecular chaperones, and the stress
734 response: evolutionary and ecological physiology. Annual Review of Physiology.
735 1999;61(1):243-82. PubMed Central PMCID: PMCHeat Shock Proteins.
736 12. Crowe KM, Newton JC, Kaltenboeck B, Johnson C. Oxidative stress responses of gulf
737 killifish exposed to hydrocarbons from the Deepwater Horizon oil spill: Potential implications
738 for aquatic food resources. Environmental Toxicology and Chemistry. 2014;33(2):370-4.
739 13. Kültz D. Plasticity and stressor specificity of osmotic and heat shock responses of
740 *Gillichthys mirabilis* gill cells. American Journal of Physiology. 1996;271(4):C1181-C93.
741 PubMed Central PMCID: PMCOsmoregulation.
742 14. Carrasco-Malio A, Díaz M, Mella M, Montoya M, Miranda A, Landaeta M, et al. Are the
743 intertidal fish highly resistant to UV-B radiation? A study based on oxidative stress in *Girella*
744 *laevifrons* (Kyphosidae). Ecotoxicology and environmental safety. 2014;100:93-8.
745 15. Baker DW, Matey V, Huynh KT, Wilson JM, Morgan JD, Brauner CJ. Complete
746 intracellular pH protection during extracellular pH depression is associated with hypercarbia

747 tolerance in white sturgeon, *Acipenser transmontanus*. American Journal of Physiology -
748 Regulatory, Integrative and Comparative Physiology. 2009;296(6):R1868-R80. doi:
749 10.1152/ajpregu.90767.2008.
750 16. Storey KB. Reptile freeze tolerance: Metabolism and gene expression. Cryobiology.
751 2006;52(1):1-16.
752 17. Churchill TA, Storey KB. Dehydration tolerance in wood frogs: a new perspective on
753 development of amphibian freeze tolerance. American Journal of Physiology.
754 1993;265(34):R1324-R32. PubMed Central PMCID: PMCDehydration.
755 18. Belkin DA. Anoxia: Tolerance in Reptiles. Science. 1963;139(3554):492-3. doi:
756 10.1126/science.139.3554.492.
757 19. Bickler PE. Cerebral anoxia tolerance in turtles: regulation of intracellular calcium and
758 pH. American Journal of Physiology. 1992;263(6):R1298-R302. PubMed Central PMCID:
759 PMCAnoxia.
760 20. Mojica EA, Fu Y, Kültz D. Salinity-responsive histone PTMs identified in the gills and
761 gonads of Mozambique tilapia (*Oreochromis mossambicus*). BMC Genomics. 2024;25(1):586.
762 Epub 20240611. doi: 10.1186/s12864-024-10471-3. PubMed PMID: 38862901; PubMed Central
763 PMCID: PMCPMC11167857.
764 21. Dyson MH, Thomson S, Mahadevan LC. Heat shock, histone H3 phosphorylation and the
765 cell cycle. Cell Cycle. 2005;4(1):e64-e-8. PubMed Central PMCID: PMCHeat Shock.
766 22. Kim JM, To TK, Ishida J, Morosawa T, Kawashima M, Matsui A, et al. Alterations of
767 lysine modifications on the histone H3 N-tail under drought stress conditions in Arabidopsis
768 thaliana. Plant & Cell Physiology. 2008;49(10):1580-8. Epub 20080908. doi:
769 10.1093/pcp/pcn133. PubMed PMID: 18779215.
770 23. Ma T, Keller JA, Yu X. RNF8-dependent histone ubiquitination during DNA damage
771 response and spermatogenesis. Acta Biochimica et Biophysica Sinica (Shanghai).
772 2011;43(5):339-45. Epub 20110328. doi: 10.1093/abbs/gmr016. PubMed PMID: 21444325;
773 PubMed Central PMCID: PMCPMC3080603.
774 24. Wang Y, Lyu Y, Tu K, Xu Q, Yang Y, Salman S, et al. Histone citrullination by PADI4
775 is required for HIF-dependent transcriptional responses to hypoxia and tumor vascularization.
776 Science Advances. 2021;7(35):eabe3771.
777 25. Wrann S, Kaufmann MR, Wirthner R, Stiehl DP, Wenger RH. HIF mediated and DNA
778 damage independent histone H2AX phosphorylation in chronic hypoxia. Biological Chemistry.
779 2013;394(4):519-28. doi: 10.1515/hsz-2012-0311.
780 26. Batie M, Fasanya T, Kenneth NS, Rocha S. Oxygen-regulated post-translation
781 modifications as master signalling pathway in cells. EMBO reports. 2023;24(12). doi:
782 10.15252/embr.202357849.
783 27. Das T, Kamle A, Kumar A, Chakravarty S. Hypoxia induced sex-difference in zebrafish
784 brain proteome profile reveals the crucial role of H3K9me3 in recovery from acute hypoxia.
785 Front Genet. 2021;12:635904. Epub 20220131. doi: 10.3389/fgene.2021.635904. PubMed
786 PMID: 35173759; PubMed Central PMCID: PMCPMC8841817.
787 28. Batie M, Frost J, Frost M, Wilson JW, Schofield P, Rocha S. Hypoxia induces rapid
788 changes to histone methylation and reprograms chromatin. Science. 2019;363(6432):1222-6. doi:
789 10.1126/science.aau5870.
790 29. Mucci S, Isaja L, Rodriguez-Varela MS, Ferriol-Laffouillere SL, Marazita M, Videla-
791 Richardson GA, et al. Acute severe hypoxia induces apoptosis of human pluripotent stem cells
792 by a HIF-1alpha and P53 independent mechanism. Sci Rep. 2022;12(1):18803. Epub 20221105.

793 doi: 10.1038/s41598-022-23650-7. PubMed PMID: 36335243; PubMed Central PMCID:
794 PMCPMC9637190.
795 30. Wijenayake S, Storey KB. Dynamic regulation of histone H3 lysine (K) acetylation and
796 deacetylation during prolonged oxygen deprivation in a champion anaerobe. Mol Cell Biochem.
797 2020;474(1-2):229-41. doi: 10.1007/s11010-020-03848-x.
798 31. Anchordoguy TJ, Hand SC. Reactivation of ubiquitination in *Artemia franciscana*
799 embryos during recovery from anoxia-induced quiescence. J Exp Biol. 1995;198(6):1299-305.
800 PubMed Central PMCID: PMCAnoxia.
801 32. Liu CL, Martone ME, Hu BR. Protein ubiquitination in postsynaptic densities after
802 transient cerebral ischemia. Journal of Cerebral Blood Flow & Metabolism. 2004;24(11):1219-
803 25.
804 33. Podrabsky J, Wilson N. Hypoxia and anoxia tolerance in the annual killifish
805 *Austrofundulus limnaeus*. ICB. 2016;56(4):500-9. doi: 10.1093/icb/icw092.
806 34. Hughes C, Mojica EA, Kültz D, Podrabsky JE. Global maintenance of histone post-
807 translational modifications during the transition into anoxia in embryos of the annual killifish
808 *Austrofundulus limnaeus*. Environ Epigenet. 2025;in press:1-32.
809 35. Van HT, Santos MA. Histone modifications and the DNA double-strand break response.
810 Cell Cycle. 2018;17(21-22):2399-410. Epub 20181114. doi: 10.1080/15384101.2018.1542899.
811 PubMed PMID: 30394812; PubMed Central PMCID: PMCPMC6342081.
812 36. Weiner A, Hsieh TH, Appleboim A, Chen HV, Rahat A, Amit I, et al. High-resolution
813 chromatin dynamics during a yeast stress response. Mol Cell. 2015;58(2):371-86. Epub
814 20150319. doi: 10.1016/j.molcel.2015.02.002. PubMed PMID: 25801168; PubMed Central
815 PMCID: PMCPMC4405355.
816 37. Riggs C, Le R, Kültz D, Zajic D, Summers A, Alvarez L, et al. Establishment and
817 characterization of an anoxia-tolerant cell line, PSU-AL-WS40NE, derived from an embryo of
818 the annual killifish *Austrofundulus limnaeus*. Comp Biochem Physiol B. 2019;232:11-22. doi:
819 10.1016/j.cbpb.2019.02.008.
820 38. Fordel E, Thijs L, Martinet W, Schrijvers D, Moens L, DeWilde S. Anoxia or oxygen and
821 glucose deprivation in SH-SY5Y cells: A step closer to the unraveling of neuroglobin and
822 cytoglobin functions. Gene. 2007;398:114-22.
823 39. Hsu KF, Wilkins SE, Hopkinson RJ, Sekirnik R, Flashman E, Kawamura A, et al.
824 Hypoxia and hypoxia mimetics differentially modulate histone post-translational modifications.
825 Epigenetics. 2021;16(1):14-27. Epub 20200701. doi: 10.1080/15592294.2020.1786305. PubMed
826 PMID: 32609604; PubMed Central PMCID: PMCPMC7889154.
827 40. Nagagaki Y, Kozakura Y, Mahandaran T, Fumoto Y, Nakato R, Shirahige K, et al.
828 Histone H3.3 chaperone HIRA renders stress-responsive genes poised for prospective lethal
829 stresses in acquired tolerance. Genes to Cells. 2024;29(9):722-34. doi: 10.1111/gtc.13140.
830 41. Liu X, Wang J, Boyer JA, Gong W, Zhao S, Xie L, et al. Histone H3 proline 16
831 hydroxylation regulates mammalian gene expression. Nat Genet. 2022;54(11):1721-35. doi:
832 10.1038/s41588-022-01212-x.
833 42. Gantner BN, Palma FR, Kayzuka C, Lacchini R, Foltz DR, Backman V, et al. Histone
834 oxidation as a new mechanism of metabolic control over gene expression. Trends in Genetics.
835 2024;40:739-46.
836 43. Mojica EA, Kültz D. A strategy to characterize the global landscape of histone post-
837 translational modifications within tissues of nonmodel organisms. J Proteome Res.

838 2024;23:2780−94. Epub 20230825. doi: 10.1021/acs.jproteome.3c00246. PubMed PMID:
839 37624673.
840 44. Stowell C, Wang L, Arbogast B, Lan J-q, Cioffi GA, Burgoyne CF, et al. Retinal
841 proteomic changes under different ischemic conditions-implication of an epigenetic regulatory
842 mechanism. International Journal of Physiology, Pathophysiology and Pharmacology.
843 2010;2(2):148.
844 45. Zager RA, Johnson AC. Renal ischemia-reperfusion injury upregulates histone-
845 modifying enzyme systems and alters histone expression at proinflammatory/profibrotic genes.
846 American Journal of Physiology-Renal Physiology. 2009;296(5):F1032-F41.
847 46. Zhou A, Simon RP, David L. Nascent proteomes of ischemic-injured and ischemic-
848 tolerant neuronal cells. International Journal of Computational Biology and Drug Design.
849 2011;4(1):40. doi: 10.1504/ijcbdd.2011.038656.
850 47. Kamakaka RT, Biggins S. Histone variants: deviants? Genes Dev. 2005;19(3):295-310.
851 doi: 10.1101/gad.1272805. PubMed PMID: 15687254.
852 48. Martire S, Banaszynski LA. The roles of histone variants in fine-tuning chromatin
853 organization and function. Nature Reviews Molecular Cell Biology. 2020;21(9):522-41. doi:
854 10.1038/s41580-020-0262-8.
855 49. Podrabsky JE, Riggs CL, Duerr JM. Anoxia Tolerance During Vertebrate Development -
856 Insights from Studies on the Annual Killifish *Austrofundulus limnaeus*. In: Padilla P, editor.
857 Anoxia. Rijeka, Croatia: InTech; 2012. p. 3-24.
858 50. Draizen EJ, Shaytan AK, Marino-Ramirez L, Talbert PB, Landsman D, Panchenko AR.
859 HistoneDB 2.0: a histone database with variants--an integrated resource to explore histones and
860 their variants. Database (Oxford). 2016;2016:baw014. Epub 20160317. doi:
861 10.1093/database/baw014. PubMed PMID: 26989147; PubMed Central PMCID:
862 PMCPMC4795928.
863 51. Singh R, Bassett E, Chakravarti A, Parthun MR. Replication-dependent histone isoforms:
864 a new source of complexity in chromatin structure and function. Nucleic Acid Res.
865 2018;46(17):8665-78. doi: 10.1093/nar/gky768. PubMed PMID: 30165676; PubMed Central
866 PMCID: PMCPMC6158624.
867 52. Park YJ, Chodaparambil JV, Bao Y, McBryant SJ, Luger K. Nucleosome assembly
868 protein 1 exchanges histone H2A-H2B dimers and assists nucleosome sliding. J Biol Chem.
869 2005;280(3):1817-25. Epub 20041030. doi: 10.1074/jbc.M411347200. PubMed PMID:
870 15516689.
871 53. Andrews AJ, Chen X, Zevin A, Stargell LA, Luger K. The histone chaperone Nap1
872 promotes nucleosome assembly by eliminating nonnucleosomal histone DNA interactions. Mol
873 Cell. 2010;37(6):834-42. doi: 10.1016/j.molcel.2010.01.037. PubMed PMID: 20347425;
874 PubMed Central PMCID: PMCPMC2880918.
875 54. Formosa T. The role of FACT in making and breaking nucleosomes. Biochim Biophys
876 Acta. 2012;1819(3-4):247-55. Epub 20110723. doi: 10.1016/j.bbagrm.2011.07.009. PubMed
877 PMID: 21807128; PubMed Central PMCID: PMCPMC3229669.
878 55. Lyu Y, Yang Y, Talwar V, Lu H, Chen C, Salman S, et al. Hypoxia-inducible factor 1
879 recruits FACT and RNF20/40 to mediate histone ubiquitination and transcriptional activation of
880 target genes. Cell Rep. 2024;43(4):113972. Epub 20240321. doi: 10.1016/j.celrep.2024.113972.
881 PubMed PMID: 38517892.
882 56. Talbert PB, Henikoff S. Histone variants at a glance. J Cell Sci. 2021;134(6):jcs244749.
883 doi: 10.1242/jcs.244749.

884 57. Boidot R, Branders S, Helleputte T, Rubio LI, Dupont P, Feron O. A generic cycling
885 hypoxia-derived prognostic gene signature: application to breast cancer profiling. Oncotarget.
886 2014;5(16):6947-63. doi: 10.18632/oncotarget.2285.
887 58. Shah S, Verma T, Rashid M, Gadewal N, Gupta S. Histone H2A isoforms: Potential
888 implications in epigenome plasticity and diseases in eukaryotes. Journal of Biosciences.
889 2020;45(1). doi: 10.1007/s12038-019-9985-0.
890 59. Wellmann S, Bettkober M, Zelmer A, Seeger K, Faigle M, Eltzschig HK, et al. Hypoxia
891 upregulates the histone demethylase JMJD1A via HIF-1. Biochemical and Biophysical Research
892 Communications. 2008;372(4):892-7. doi: https://doi.org/10.1016/j.bbrc.2008.05.150.
893 60. Fabrizio P, Garvis S, Palladino F. Histone methylation and memory of environmental
894 stress. Cells. 2019;8(4):339. doi: 10.3390/cells8040339.
895 61. Kim J, Lee H, Yi SJ, Kim K. Gene regulation by histone-modifying enzymes under
896 hypoxic conditions: a focus on histone methylation and acetylation. Experimental & Molecular
897 Medicine. 2022;54(7):878-89. Epub 20220722. doi: 10.1038/s12276-022-00812-1. PubMed
898 PMID: 35869366; PubMed Central PMCID: PMCPMC9355978.
899 62. Brustel J, Muramoto T, Fumimoto K, Ellins J, Pears CJ, Lakin ND. Linking DNA repair
900 and cell cycle progression through serine ADP-ribosylation of histones. Nature Communications.
901 2022;13(1). doi: 10.1038/s41467-021-27867-4.
902 63. Marnett LJ. Oxyradicals and DNA damage. Carcinogenesis. 2000;21(3):361-70. doi:
903 10.1093/carcin/21.3.361.
904 64. Poltronieri P, Miwa M, Masutani M. ADP-ribosylation as post-translational modification
905 of proteins: Use of inhibitors in cancer control. Int J Mol Sci. 2021;22(19):10829. doi:
906 10.3390/ijms221910829.
907 65. Bartlett E, Bonfiglio JJ, Prokhorova E, Colby T, Zobel F, Ahel I, et al. Interplay of
908 histone marks with serine ADP-ribosylation. Cell Rep. 2018;24(13):3488-502.e5. doi:
909 10.1016/j.celrep.2018.08.092.
910 66. Mohapatra J, Tashiro K, Beckner RL, Sierra J, Kilgore JA, Williams NS, et al. Serine
911 ADP-ribosylation marks nucleosomes for ALC1-dependent chromatin remodeling. Elife.
912 2021;10. Epub 20211207. doi: 10.7554/eLife.71502. PubMed PMID: 34874266; PubMed
913 Central PMCID: PMCPMC8683085.
914 67. Martinez-Zamudio R, Ha HC. Histone ADP-ribosylation facilitates gene transcription by
915 directly remodeling nucleosomes. Mol Cell Biol. 2012;32(13):2490-502. Epub 20120430. doi:
916 10.1128/MCB.06667-11. PubMed PMID: 22547677; PubMed Central PMCID:
917 PMCPMC3434492.
918 68. Bhagat TD, Von Ahrens D, Dawlaty M, Zou Y, Baddour J, Achreja A, et al. Lactate-
919 mediated epigenetic reprogramming regulates formation of human pancreatic cancer-associated
920 fibroblasts. eLife. 2019;8:e50663. Epub 20191101. doi: 10.7554/eLife.50663. PubMed PMID:
921 31663852; PubMed Central PMCID: PMCPMC6874475.
922 69. Zhang D, Tang Z, Huang H, Zhou G, Cui C, Weng Y, et al. Metabolic regulation of gene
923 expression by histone lactylation. Nature. 2019;574(7779):575-80.
924 70. Zhang W, Tan X, Lin S, Gou Y, Han C, Zhang C, et al. CPLM 4.0: an updated database
925 with rich annotations for protein lysine modifications. Nucleic Acid Res. 2022;50(D1):D451-D9.
926 doi: 10.1093/nar/gkab849. PubMed PMID: 34581824; PubMed Central PMCID:
927 PMCPMC8728254.
928 71. Fernandez-Capetillo O, Lee A, Nussenzweig M, Nussenzweig A. H2AX: the histone
929 guardian of the genome. DNA Repair. 2004;3(8-9):959-67. doi: 10.1016/j.dnarep.2004.03.024.

930 72. Xiao A, Li H, Shechter D, Ahn SH, Fabrizio LA, Erdjument-Bromage H, et al. WSTF
931 regulates the H2A.X DNA damage response via a novel tyrosine kinase activity. Nature.
932 2009;457(7225):57-62. doi: 10.1038/nature07668.
933 73. Rossetto D, Avvakumov N, Côté J. Histone phosphorylation. Epigenetics.
934 2012;7(10):1098-108. doi: 10.4161/epi.21975.
935 74. Root L, Campo A, Macniven L, Con P, Cnaani A, Kültz D. A data-independent
936 acquisition (DIA) assay library for quantitation of environmental effects on the kidney proteome
937 of *Oreochromis niloticus*. Mol Ecol Resour. 2021;21(7):2486-503. doi: 10.1111/1755-
938 0998.13445.
939 75. Kong AT, Leprevost FV, Avtonomov DM, Mellacheruvu D, Nesvizhskii AI. MSFragger:
940 ultrafast and comprehensive peptide identification in mass spectrometry-based proteomics. Nat
941 Methods. 2017;14(5):513-20. Epub 20170410. doi: 10.1038/nmeth.4256. PubMed PMID:
942 28394336; PubMed Central PMCID: PMCPMC5409104.
943 76. Benjamini Y, Hochberg Y. Controlling the false discovery rate: A practical and powerful
944 approach to multiple testing. J R Statist Soc B. 1995;57:289-300. doi: 10.1111/j.2517-
945 6161.1995.tb02031.x.
946 77. MacLean B, Tomazela DM, Shulman N, Chambers M, Finney GL, Frewen B, et al.
947 Skyline: an open source document editor for creating and analyzing targeted proteomics
948 experiments. Bioinformatics. 2010;26(7):966-8. Epub 20100209. doi:
949 10.1093/bioinformatics/btq054. PubMed PMID: 20147306; PubMed Central PMCID:
950 PMCPMC2844992.
951 78. Du P, Zhang X, Huang C-C, Jafari N, Kibbe WA, Hou L, et al. Comparison of Beta-
952 value and M-value methods for quantifying methylation levels by microarray analysis. BMC
953 Bioinformatics. 2010;11:587. doi: 10.1186/1471-2105-11-587.
954 79. Chappell K, Graw S, Washam CL, Storey AJ, Bolden C, Peterson EC, et al. PTMViz: a
955 tool for analyzing and visualizing histone post translational modification data. BMC
956 Bioinformatics. 2021;22(1):275. doi: 10.1186/s12859-021-04166-9.
957 80. Wickham H. Elegant Graphics for Data Analysis. New York: Springer-Verlag; 2016.
958